Enhancing Bridge Weigh-in-Motion System by Accurate Observation of the Velocity and Axle Spacings of Moving Truck Using a Geophone Sensor

by

Maedeh Mirzaei

A Thesis submitted to the Faculty of Graduate Studies of
The University of Manitoba
in partial fulfillment of the requirements of the degree of

MASTER OF SCIENCE

Department of Civil Engineering
University of Manitoba
Winnipeg

Abstract

Bridges are a critical element of an economy's transportation network. Most old bridges, however, have some structural or geometrical flaws. Structural health monitoring (SHM) systems, including bridge-weighing-in-motion (BWIM) devices, have evolved in recent years to identify and analyze the structural behaviour of old bridges with the aim of extending the lifetime of the structures. Heavy loads are one of the factors that should be considered and analyzed for bridge structures. It is one of the significant obstacles that bridges face, as they cause vibration, which leads to bridge decks cracking and steel girders to fatigue. Understanding the Gross Vehicle Weight (GVW of a truck) and Axle weights determines the strength and the bridge deck and girders' load-bearing capability. The GVW is computed using the bridge Weigh in Motion (BWIM) system. This paper explores a new methodology utilizing geophones to estimate the velocity, number of axles, axle spacings, and individual axle weights of loads moving over a bridge. The main finding is that geophones can accurately determine the truck velocity and axle spacing based on the test data set conducted in the actual and laboratory model bridge. Therefore, the truck's complete configuration—an essential component for accurately assessing bridges' strength and weight-carrying capacity—will be defined by the truck's velocity, axle spacing, and GVW.

Acknowledgements

First and foremost, I would like to express my deep gratitude to my supervisor, Professor Aftab Mufti, for his ongoing assistance and guidance, which were indispensable to the accomplishment of this project. His advice always helped me to find the right direction. It enabled me to flourish both academically and individually. Working under his supervision was a privilege.

My deepest gratitude is extended to Professor Douglas Thomson for his unconditional support and assistance in developing and organizing the research project. His teachings and support have allowed me to grow as a researcher. He was constantly available to assist and patiently provided explanations. Working with him was a great pleasure.

Many thanks to Professor Jonathan Regehr for serving on my committee and for his constructive comments on the thesis. Special thanks to Professor Baidar Bakht for his knowledge and help during the research work and the defence session. I would also like to acknowledge Dr. Karim Helmy and Dr. Basheer Algohi for their help. Special thanks to Charleen Choboter for providing me with support and coordinating everything I needed during the research.

Special acknowledgements are given to my family for their unconditional love and support as always, especially during the challenging time of completing the research.

TABLE OF CONTENTS

LIST OF TABLES

LIST OF FIGURES

1. Introduction

1.1 Overview

Bridges are an essential part of the transportation and infrastructure network. The bridge's structural strength assessment is based on traffic monitoring. One of the critical elements in traffic monitoring of bridges is heavy truckloads, which cause fatigue in steel girders and deterioration in concrete bridge decks. Preventing the failure of bridges due to an increase in traffic loads will be an essential factor that should be considered further (Mufti & Helmi, 2019). Therefore, observing the vehicle loads that pass over the bridges performs a significant role in planning the bridge networks for monitoring and maintaining the bridge structures. Ongoing maintenance, infrastructure planning, and implementation of loading capacity can all be guided and improved by accurately determining the vehicle's gross weight, velocity and axle weights when using a bridge as a scale (Helmi et al., 2014; Faraz, 2020). This study proposes a novel technology that uses a geophone sensor to calculate velocity and axle spacing significantly more accurately than existing approaches.

This introduction chapter will focus on the background and context, followed by the research aims, objectives, significance, limitations, and overall thesis layout.

1.2 Background and context

In the past, the most frequently used technique to track vehicle weight on the roadway was weighing statically in stations. However, stationary scales require that every vehicle be weighed before leaving the roadway, even though they provide exact weight measurements. Nowadays, based on structural health monitoring techniques, some methods like a Bridge-

Weight-In-Motion system (BWIM) were designed to estimate the weight of heavy vehicles without interrupting the traffic and stopping vehicles on the highway. Weigh-in-motion (WIM) and bridge weigh-in-motion (BWIM) are substitutes for static weigh stations. The WIM systems are frequently installed beneath a roadway and will calculate the weight of trucks when it passes that spot. Today, BWIM systems can be installed on most bridge types.

Additionally, they have a lower sensitivity to dynamic systems brought on by unlevel surfaces. Fig 1.1. depicts the primary data-stream components of a BWIM system, from the data acquisition system to event recognition, observation of the truck configuration, and weight calculation. The BWIM has two final elements, gross vehicle weights and individual axle weights. Three sets of parameters must be determined: influence lines, global events, and truck specifications to achieve the main components of the BWIM system (MacLeod & Arjomandi, 2022a). The Global events are indicated through weighing sensors. These sensors' ability to collect high-quality data is influenced by the bridge's design and the type and location of the used sensor. The influence line parameter is predicted with an analytical function that must be calibrated using the structure's response to calibration vehicle(s) with known characteristics to reliably predict influence lines, which are inherent aspects of a bridge structure. Truck specifications are also commonly done using detector sensors to identify the axles of moving trucks. These sensors measure local events to calculate the vehicle's speed and axle spacing. The identification of vehicles among these three parameters is a research-intensive sector with many opportunities for advancements in sensor design, model, and location, as well as in processing techniques for precisely identifying vehicle attributes. The identification of vehicles among these three parameters is a research-intensive sector with many opportunities for

advancements in sensor design, model, and location, as well as in processing techniques for precisely defining vehicle characteristics. The potential of some of the most recent developments in BWIM technologies and vehicle identification will be further discussed in Chapter 2. However, there are still some gaps and uncertainties in identifying the vehicle's configuration, which limits the ability to estimate the individual axle weights precisely and hence define the load capacity of bridges. Inaccuracy in truck configuration information contains multiple concerns, including collapse, structural failure, and project financial difficulties. This research aims to boost the accuracy of calculations and outcomes of truck identifications by proposing a novel approach to identifying a vehicle's configuration. The research outcomes will show that this method could significantly enhance the accuracy of calculations rather than the previous approaches.

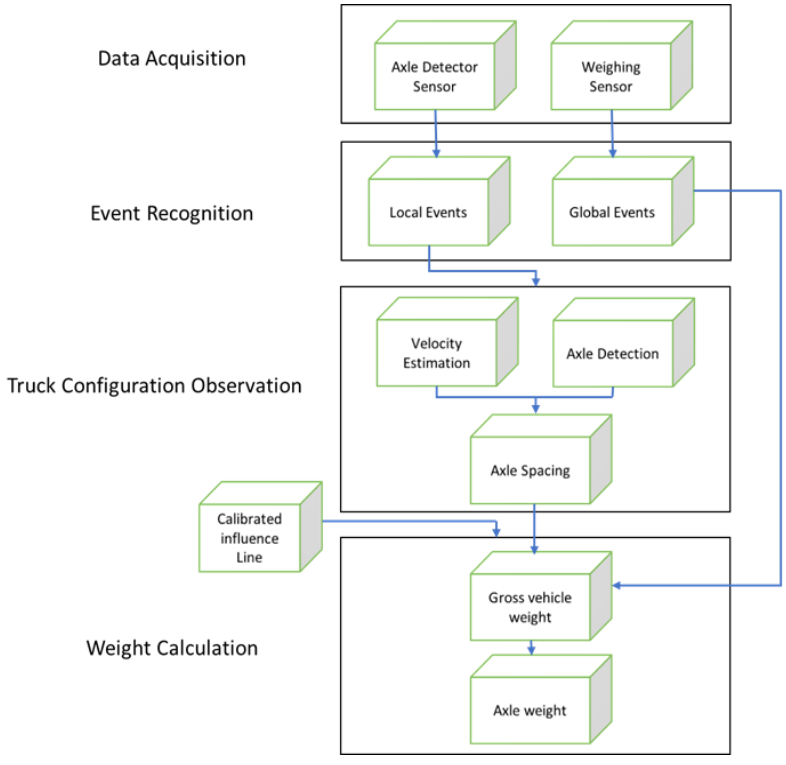

Fig 1.1: Data Stream in BWIM

1.3 Research aims and objectives

Structural Innovation and Monitoring Research Group (SIMTReC) developed a BWIM system for calculating gross vehicle weights. The system is extended to include estimates for axle weights and configuration. Critical to this extension is having a means to accurately estimate vehicle velocity, the axle number, and the distance between axles. The novel work presented here explores using a geophone sensor as an axle detector sensor mounted over a bridge bearing to calculate vehicle velocity, axle number and distance between axles. The geophone is a sensor that outputs a voltage in response to the velocity of the sensor (Bahrani et al., 2020). The geophone measures the dynamic displacement of the compressible bridge bearing, which is compressed by tire loads passing over the expansion joints. It is not required the geophone be precisely placed under the tire path for velocity and axle spacing calculations. The bearing's vertical velocity measurements determine the time at which tire loads pass over the bearing. The vehicle speed, configuration, and distances can be estimated. An algorithm was devised for filtering the signals to remove unnecessary noise and vibrations from the raw geophone signal. The results presented at the end of Chapters three and four will demonstrate that the geophone can be used as an axle detector in the BWIM system, which considerably improved the level of precision in the velocity and axle spacing computations. Along with precision in the calculation, it is also easy to be installed. Unexpectedly, just one geophone sensor is needed as it can detect signals from bearings at both ends of a supported span.

The remaining part of this research is divided into various chapters, each of which will detail the proposed approach and the other studies in the field. In chapter one, the context of

the study is introduced. The research objectives and aims have been identified, and the value of such research has been argued.

Chapter two will review the existing literature to identify critical skills and development approaches and strategies within the BWIM system and the vehicle identification approaches.

In chapter three, the theoretical frameworks in the field will be presented. The experiments conducted in the actual bridge for estimating and validating the novel method and results of vehicle configuration, axle numbers, velocity, and axle spacings of the trucks will be described, analyzed, and presented in detail.

In chapter four, the theoretical frameworks in the laboratory will be discussed. The approach of estimation and validation on a bridge model in the structural health monitoring laboratory, the results of the model trucks' speed, axle numbers, and axle distances will be presented.

The last chapter will describe the conclusion and summary of the outcomes received from this research and the suggested further research.

2. Literature Review

2.1 Introduction

Controlling and monitoring overloaded vehicles has a significant role in preventing bridges from fatigue that causes collapse into structures. It is essential to manage these vehicles to maintain the modern transportation system and increase the life serviceability of bridges. Some technologies, such as weighing statically on stationary scales and weigh-in-motion (WIM) techniques, are offered. The WIM method aims to measure the vehicle's weight under normal traffic conditions. This method had some limitations as the devices should be installed on the road's surface. As a result, the other proposed method is called the bridge weigh-in-motion (B-WIM) system. In this method, the instrumented bridge is used as a weighting scale to calculate the weights of the vehicle. The durability of the BWIM over the WIM is because of installing sensors under the bridges without any traffic interruption, which makes BWIM better than WIM. BWIM has a safe and easy installation. In addition, the results from BWIM are more accurate than those from the WIM. It directly affects the axle weight estimation process since the contact area in WIM between the vehicle tires and the embedded sensors on the pavement surface is insufficient for the completed oscillation of the axle force cycle. However, BWIM can record the complete cycle of the difference axle force from the bridge responses. After many experiments on BWIM algorithms, such as the static and dynamic algorithms, the typical instrumentations using the sensors for identifying and detecting axles and measuring the strain were developed for the BWIM system. Still, significant efforts are made to highlight the problems associated with using bridge weigh-in-motion technology which will be described later in this research.

The Bridge Weigh in Motion System uses strain measuring instruments underside the bridges without any traffic interruption during the installation. In BWIM, there is a theoretical possibility of minimizing the effects of dynamic loads as vehicles have a longer time in contact with the bridges. However, the main drawback of the BWIM system is that the essential part of the measurement system is the bridge structures. The weight measurement systems need the responses from the bridges continuously to estimate the speeds. The following sections discuss the various BWIM and axle detection development strategies since the early stage of developing the BWIM system.

2.2 Early B-WIM Development:

Fred Moses and George Globe first invented BWIM in the 1970s in Us. Then Rob Peters successfully deployed it in Australia with a more accessible culvert version.

Early interests and achievements:

Using the electronic devices in BWIM was presented in 1961 in Michigan State Highway Department for the first time. They installed the platform load cells on the lane adjacent to the station, where they estimated the weights. In 1968 Lee and Nasser applied an early WIM system, design, and construction in Texas. Their system was not dependent on the traffic line condition and could estimate the velocity, length, number of axles, axle spacings and tire weights. Many investigations have been conducted to produce the WIM system in many aspects, such as portability and flexibility.

Goble, Moses, and Pavia:

Goble, Moses, and Pavia researched BWIM at Reserve University with sponsorship from the Federal Highway Administration and the Ohio Department of Transportation. The goal was to gather enough information to statistically analyze the fatigue life of bridges. For developing the histories of the strain gauges measurement process, the research was done in Ohio for ten girder slab highway bridges that were instrumented by strain gauges which were collected data under normal traffic conditions for a day or half. The pressure range was symmetrically documented for the first time in this project for the closely spaced trucks and headways of the trucks. It was determined that bridges might be utilized as a new scale based on the findings of this experiment and the data comparison between bridges and the weight station data (Richardson et al., 2014a).

Fred Moses (1979):

To weigh trucks crossing a bridge at maximum highway speeds, Moses and Goble invented B-WIM in 1979 in the US. For the first time in 1979, Fred Moses proposed the methodology to calculate the axle weight of trucks using the measured histories from the bridge strain (Moses, 1979);(L. Yu & Chan, 2007). He noted that one of the benefits of utilizing this method versus pavement-based weight-in-motion devices is the longer interfacial time between the bridges and the vehicles. This longer time allows more recorded data to reduce the dynamic effects with better statical analysis. However, it cannot realize and analyze the closely spaced axles due to the longer contact time. The Moses system has four parts: A Button Box, Tape Switches, Strain Transducers, and an Instrument Van. A Button Box was placed before the bridges. The operator signalled the system that a truck was arriving by pressing the button when the truck was seen.

Double tape switches were placed on the surface in a similar direction at a predetermined length to measure truck speed, axle lengths, and axle locations. A tape switch in the third position was also utilized to command the device to record the strain data for a specific period shortly before the bridge. This estimation was based on the truck that traversed the bridge at the slowest speed. Two metallic strips kept separate from one another made up a tape switch. The switch was activated when an axle crossed it because a tire pressing on the tape switches caused the metallic strips to interact directly. Strain gauges are positioned on each girder's bottom flange in a line perpendicular to the bridge's direction. The best place was advised to be in the middle of the span. The magnetic tape was used to independently capture the strain data for each gauge. After gathering, the processing program added the signals from each girder individually. The strain transducers and traffic detectors sent signals to the van parked underneath the bridge. The digital traffic lights continued to function as the signal of strains was transmitted straight to the computer. The output of signals was recorded on magnetic tape using a minicomputer system's analog-to-digital converter. A technique known as "weighing in motion" is used to record the structural response and identify the load that was caused. The effect line of the bridge can be identified using structural analysis or a calibration vehicle with statically known axle weights. Moses suggested using a single short span (under 60 feet) to measure axle weight individually, whereas for estimating gross vehicle weights, a longer span (over 80 feet) was preferable (Y. Yu et al., 2016b).

Rob Peters in Australia (1984):

Early in the 1980s, similar systems as Moses were created in Australia by Peters, primarily for culverts. In 1984, Peters proposed using the instrumented bridges as a sizeable dynamic

scale to compute the gross vehicle weight and axle of the trucks that passed over the bridges. In 1980, the reinforced deck of the Maddington Bridge crossing the Beechboro Gosnells Highway was equipped with electrical resistance strain gauges. The gauge readings for the strain were too small to be accurately monitored. Therefore, the mechanical strain amplifier (MSA) was created. The MSA values were more than the strain. It is challenging to get vehicle axle weight spectra, even though they are crucial for transportation studies, paving, and bridge construction. AXWAY is a proposed method by Peters to monitor cars' axle weights while moving at highway speeds and uses bridges as substantial dynamic scales (Richardson et al., 2014b).

The velocity of trucks, axle distancing, and the bridge's response to the vehicle's strain are all measured and recorded using an Australian Road Research Board (ARRB) data-gathering system. The axle weights are then calculated using this data, which are subsequently sent to a mainframe computer for further processing. A vehicle crossing a bridge causes a strain influence line to form, which accurately indicates the vehicle's gross weight and individual axle. Peters points out that one of the biggest challenges in the execution of AXWAY was the creation of axle detectors. They must be dependable, waterproof, and strong. It was found that while air hoses accurately detected speeds, they were inefficient at numbering axles. It was discovered that photo-electric cells, which send a light beam over the road, did not have good outcomes. For the AXWAY system, a third method utilized burglar alarm mats that were 95% reliable and sufficient. Since AXWAY was an operating solution, gathering large amounts of data was costly. Peters then created a new system named CULWAY (Peters et al., 1986); (Richardson et al., 2014b). It weighed a vehicle's axle as it crossed a culvert. One of the significant sources of

errors for bridge-based WIM systems is the dirt in the culvert and the pavement. It is worth mentioning that culverts are not subject to the related vehicle dynamic pressures and abutments.

European B-WIM Developments:

This part focused on WAVE and COST 323, two major European research efforts that provided funding for several significant B-WIM advancements in the late 1990s. B-WIM did not take off outside of Australia until the late 1990s. In the interest of enhancing scientific and technological research collaboration across Europe, the COST 323 initiative served as an international framework. The first on-surface truck WIM cooperative action in Europe resulted in two conferences, numerous extensive BWIM tests, and a Weigh in motion system standard. Additionally, the European project funded considerable research into WIM generally and B-WIM in the late 1990s (Lydon et al., 2016). The three following sub-sections provide a summary of the work's findings. Axle detection techniques are first employed to determine vehicle velocity, axle location, and spacing. The second one is the measurement of strains. A surface of influence lines can be created using strain values from several transverse locations on the bridge. The B-WIM accuracy is further enhanced by axle dynamic form load on the bridge. The classification of WIM systems' correctness according to COST 323 was one of the most significant advances. As a result, various B-WIM configurations, algorithms, and systems may be directly compared. Because NOR did away with the necessity for surface sensors, it was also a huge advancement. The portability of B-WIM equipment and its capacity to be installed with little to no disruption to traffic and restricted driver visibility are significant advantages over pavement WIM deployments (Lydon et al., 2016).

2.3 Axle Detection Developments

In earlier B-WIM systems, the pavement-embedded low-grade piezoelectric sensors were either permanent low-grade piezoelectric sensors or permanent tape switches with removable pneumatic hoses. It would be possible to estimate the axle spacing, position, and speed of cars crossing the bridge using two axle detectors, one in each lane. (Y. Yu et al., 2016b). In France, axle identification was made using measured stresses in stiffeners longitudinally spaced on an orthotropic bridge deck (Zhao & Uddin, 2010). A "free of axle detectors" installation, often known as "nothing on the road" (NOR), does not interrupt traffic. It is being installed concurrently but is hidden from view from vehicles travelling across a bridge. In addition, integrated slab bridges employed it (E. J. O'Brien et al., 1999). Some experiments have been conducted to enhance the accuracy of velocity and axle weight calculations. The more the velocity calculation is accurate, the more the axle weights estimation becomes accurate. The optimization procedure can involve velocity, which enhances accuracy but necessitates an intense initial calculation. When axles are moving overhead, wavelet domain analysis is used to find anomalies in strain histories (Chatterjee et al., 2006). This better knowledge of axle position at certain times causes more precise velocity measurements. Another method to determine the velocity, similar to Dempsey's concept, is correlating the longitudinal strain from the two vertical sites on the bridge.

Japanese B-WIM Efforts:

Based on Moses's idea, Miki introduced nothing on the road system for bridges with steel girders in Japan in the 1980s (N. B. Wang et al., 2017). Stiffeners instrumented vertically on the web plate were used in determining axles in this method. Although this technique implies

cracks exist, the crack of reinforced slab crack holes was sensitive enough to detect axle loads (E. O'Brien et al., 2013).

Identification of moving force and dynamic model

O'Connor and Chan create a dynamic B-WIM algorithm in 1988s to recognize high-impact trucks on bridges with short spans. Additionally, to the vehicle's static axle weights when traversing a bridge, (Oskoui et al., 2020) propose a B-WIM technique that estimates the bridge amplitude dynamic vibration. Model superposition was used to calculate a bridge's dynamic reaction to a moving fixed axle force (Zhao & Uddin, 2010). A theoretical study's estimation of the damping ratio was set at 2%, and an experimental study's measurement of the natural frequency was based on a theoretical study's measuring the frequency using the bridge's shape. From the anticipated displacements for the experimental investigation, projected bridge stresses were estimated at a single longitudinal location. In both trials, the static model (Moses) load identification method was more accurate than the dynamic axle load identification technique. Due to the truck's rolling and bouncing, the forces applied through the truck's tires to a bridge are inconsistent over time (Maros & Juniar, 2016). They discovered a connection between the degree of axles and the number of areas where sensors were needed. This method is not appropriate for supported bridges. Several researchers theorized and experimentally tested to theoretically identify the B-WIM algorithms and bridge measurement differences using data from four bridge sites (Law & Fang, 2001); (González, A., and O'Brien, 1998); (Zhao et al., 2014) ; (Zhu & Law, 2001); (Y. Yu et al., 2016b). It is discussed how dynamics and a large number of sensors impact B-WIM systems' precision.

Moses' calculations fail to account for axle spacing concerning the bridge span. They show through simulations and field tests that employing enhances the equation conditioning. The Tikhonov method may lead to significant accuracy gains. Following this, (Wu & Law, 2010) suggested calibration options for a B-WIM technique based on Moving Force Identification. (Obrien et al., 2010) provide a "filtered measured" method for approaching bridge weight in motion. The strain signal is subjected to Moses' algorithm following the removal of dynamic effects. This approach differs from others in that the calibration truck signal is subjected to the same filter processing as the other signals. Regularized moving force identification is a complex and promising method that may be used to determine the axle force time(Ojio et al., 2016) histories travelling across a bridge from observed bridge strain histories (Rowley et al., 2009). The time histories of axle force may be used to derive the static axle forces (or weights). The approach includes using a finite element model to formulate the bridge's equations of motion. The bridge strain measurements' observed frequencies and damping ratios can be used to modify the model (Rowley et al., 2009). Modal superposition is utilized to reduce the number of required equations. Tikhonov regularisation improves poorly conditioned solutions, and dynamic programming is used to estimate the ideal projected axle weights to diminish observed and expected stress differences. The use of synthetic data demonstrates that noises less influence the accuracy of the moving force identification (MFI) methodology rather than the B-WIM method proposed by Moses. The MFI method had an accurate axle spacing calculation based on strain data.

Hidden System in BWIM

B-WIM systems may be installed below the bridge deck to be hidden entirely from oncoming traffic. In most cases, the static weigh staff is situated downstream from the bridge, lowering the possibility that truckers may draw a link between the bridge and the static weigh staff. There is no visible weight-measuring equipment when crossing the bridge, but pre-selection systems often require a camera positioned at the bridge location, which could make the vehicle suspicious.

Communication with Weigh Crew

A precise explanation must be sent to the downstream weigh staff for a vehicle to be removed from the flow of traffic to be weighed statically after the B-WIM system has weighed and considered them overweighted trucks. One approach is to send a car picture transverse the bridge through the smartphone network. An arrival time was calculated according to the bridge and the position of static weighing distances. The image and data on the information about the truck's specifications may then be used to identify the truck model and axle numbers quickly. Cell phones sent the picture and other B-WIM data from the station site to the BWIM site. It is also possible to station a person at the bridge site while static weighing is being done to use B-WIM data for pre-selection. Every time a large vehicle passes the bridge, its type, shape, and colour are noted together with its GVW, the transit date, and the time. After obtaining information on the car by CB radio or another manner, the weigh crew will decide which vehicle needs to be stopped and weighed (Y. Yu et al., 2016a).

SiWIM

The only B-WIM system available in the market is SiWIM, developed and manufactured in Slovenia by CESTEL. For calculating the axle loads and GVW of trucks traversing the bridge,

SiWIM uses Moses' method. The system supports NOR and enables the installation of a camera for taking pictures of large trucks. Once access to the bridge's underbelly is granted, installing the system is simple. Pre-selection can start the next day when the sensors have been installed and the system calibrated. The components of the SiWIM system are a temperature sensor, strain sensors, a cabinet that holds the system engine, and additional add-ons like a camera and router. (Y. Yu et al., 2016a).

Axle detector optimization methods

Some factors cause BWIM system uncertainties, such as the dynamic effects of vehicles passing the bridges, the sensitivities of electrical sensors, and inaccurate influence lines. One of the significant problems in Moses's algorithm is the dependency of this algorithm in accurately finding the influence lines. The BWIM system has a high potential in calculating the gross vehicle weight because the estimation process is based on the calculated response assigned to the total vehicle weight. However, BWIM has not itself have the ability to calculate the individual axle weight. Most BWIM systems are based on estimating the strains. Due to the low dynamic effect attributed to moving force and sharper influence lines, it is appropriate for bridges with orthotropic decks, concrete beam slabs, and integral concrete slabs with short and medium spans ((Zhao et al., 2014); (Carraro et al., 2019); (Bao et al., 2016); (Lydon et al., 2017); (Helmi et al., 2015). Recently, the BWIM system was developed especially for long and short-span bridges using electrical devices such as accelerometers and strain gauges. (Sekiya et al., 2018b); (McCrum et al., 2018). Although the strain gauges have more accurate results due to the displacement influence lines based on the acceleration measurements being smeared and having no recognizable peak, accelerometers have lower cost, easier installation, and lower

noise. (Sekiya et al., 2018b). The other method proposed by (Hansen P.C., 1994) performed better approaches than Moses' Algorithm in finding the axle weight for closely spaced axles. In this method, the closely spaced axles are considered a group of axles. Their load was assumed to be a shared load for the axle group (Hansen P.C., 1994). The moving force identification method is proposed to improve the axle weight identification process. (H. Wang et al., 2017); (Liu & Yu, 2019); (Chen et al., 2019). However, it has an issue in real-time applications requiring a full 3D model of the bridges.

2.4 Development in Axle detector sensors:

Axle detecting techniques from the past employed axle detectors that need installation directly on the pavement leads to poor durability and necessitates blocking lanes of traffic. The weigh-in-motion in Europe introduced the free axle detector (FAD) technology to address the drawbacks of these conventional techniques (Christian et al., 2015). This system locally estimates the bending strains and is the most suitable for orthotropic decks and short-span bridges (Zhao et al., 2014); (Kalin et al., 2006). One of the shortcomings of FAD systems is their sensitivity to tire position, which results in an error in strain bending computation when the tire's location changes as it passes over the bridges (Dowling et al., 2012). Another disadvantage of this approach is computing loads for long-span bridges, as it is challenging to verify that all tire places in the bridge have the associated sensors underneath. As a result of limitations associated with the FAD system and bridge characteristics, numerous sensing technologies have been developed to identify axles' position and distance, independent of the characteristic of bridges. (Bao et al., 2016) proposed the idea of using the shear strain to

calculate the weight of the trucks. One of the new systems that Lydon proposed in 2017, based on the previous method, utilized a bearing strain with fibre optical sensors (FOS) as an axle detector in the NOR BWIM system to increase accuracy (Lydon et al., 2017). Other innovative techniques were proposed using a camera on the side of the road to measure the axle distances (Ojio et al., 2016). Using Microphones also was presented to record the acoustic waves produced when the truck's wheels passed expansion joints. It was considered a contactless technology to detect and dete rmine the local events of the vehicles that transverse over the bridges (Algohi et al., 2018). Another method of enhancing BWIM in determining the closely spaced individual axles' weight is proposed to improve the linear optimization accuracy problem of the BWIM system using acceleration measurements, especially for long-span bridges. (Mustafa et al., 2021a). The suggested method uses acceleration data from microelectromechanical system accelerometers (MEMS) as bridge displacement responses to calculate the vehicle velocities, axle numbers, and spacings. Installed MEMs (Microelectromechanical system accelerometers) at the leaving spans, leading to a low bridge dynamic response and extremely sharp peaks matching axle position and number of vehicles. It then uses the identifying peaks in signals to determine when the vehicles entered and left the bridges. (Mustafa et al., 2021b; Sekiya, 2019; Sekiya et al., 2018a). Although the results of the above methods are impressive, they are inevitably inaccurate due to noise, road imperfections, and administrative issues. Numerous signal processing techniques, such as different filtering methods, were proposed to increase the FAD sensors' ability to detect challenging environments. One of them was the low pass filtering method that filtered the signal twice, one with the largest length and the other one shortest distance in the axle group. The difference

was examined for axles (Kalin et al., 2006). The wavelet analysis is the other filter proposed in the FAD system to determine the speed of vehicles and the axle distances based on transforming signals (Chatterjee et al., 2006). The same approach of using the transforming signal, based on the detection of global events, provided the BWIM technology with the new idea to determine axles and vehicle specifications using the weighing sensors (Y. Yu et al., 2017a). However, this method was not practically verified. Recently, the new method of using the Hybrid strain accelerometer sensors. The accelerometer sensors were used to determine the local events for identifying the velocity and truck configuration. This investigation revealed that, compared to FAD-based systems, the suggested hybrid system using the global accelerometer produced a BWIM system with enhanced accuracy. The axle spacing calculation based on this research had the lowest error, equal to 1% (MacLeod & Arjomandi, 2022a).

The table below summarizes various methods of improving axle detection information in the BWIM system to improve the BWIM System's local event identification.

Table 2.1. Summary of Some of the Recent Methods in Detecting Trucks' Velocity and Axle Spacings

Axle Detection Methods in BWIM	Citation	Accuracy
Portable BWIM Using Accelerometer Only Comments: Acceleration at the vertical stiffener to detect trucks axle numbers and speed by using just three calibrated trucks. Small, Not Expensive, Low Power Amount. Attached at the longitudinal center of the lower flange	(Sekiya et al., 2018a)	Just mentioned MEMS accelerometer sensors can accurately identify truck's velocity and axle spacings. This research was not able to accurately detect GVW and truck's individual axle weights.

Iterative linear optimization method for bridge weigh-in-motion systems using accelerometers Comments: Three four-axle vehicles were used in this experiment	(Mustafa et al., 2021a)	Accurate Measurement of axle spacings with maximum positive error 1% and maximum negative error -4.1%. It could calculate the closely axle spacings with error less than its previous similar methods.
Hybrid strain accelerometer sensors Comments: Accelerometers were added to strain based BWIM system. Accelerometers are not able to give the velocity of the bridge response directly.	(MacLeod & Arjomandi, 2022b)	Lowest error 1 % Standard deviation 4 % in axle spacing calculation. Velocity average error -1.6 % and standard deviation 2.5 %.
Strain based Free Axle Detector BWIM System Comments: Sensitivity of this method to tire position, which results in an error in strain bending computation when the tire's location changes as it passes over the bridges.	(MacLeod & Arjomandi, 2022a)	Lowest error 5%, Standard deviation 11 % in axle spacing calculation. Velocity average error -1.9 % and standard deviation 10.8 %.
Equivalent Shear Force Method (ESF) Comments: Nothing on the road BWIM system that does not require an additional axle detector sensor. By using the flexural strain signals from the weighing sensors, it estimated the trucks' velocity and axle spacings. Strain gauges attached under the bridge on the girder which prevent traffic interruption.	(Deng et al., 2018)	The total average and standard deviation error for axle spacings and velocity calculation were not reported for the results in this research.
Fiber Optic Sensors (FOS) Comments: Used fiber optic sensor to improve the axle detection; this is the combination of nothing on-road system and alternative methods of calculating the strain.	(Lydon et al., 2017)	Axle Spacing and velocity mean, and standard deviation error were not reported.

Vehicle axle identification using wavelet analysis of bridge global responses Comments: Detect axle information from the global response of the bridge. It needs a high sample rating.	(Y. Yu et al., 2017b)	The axle spacing percentage error results for each truck were changed and be more accurate with increasing the sample rating. The total average error was not reported for the tested results.
Camera Using Comments: Contactless technology. Uncertainties might happen due to practical issues, interference from the sun, maintenance on lenses, coverings on the camera, for processing real time large amount of information were required, high power computer running also is necessary	(Ojio et al., 2016)	Axle Spacing and Velocity were not reported.
Microphones to record the acoustic waves Comments: Contactless technology. It compared the final results with the camera results they used as a truth. The method could have an inaccuracy due to noise, road imperfections, and practical issues.	(Algohi et al., 2018)	The maximum absolute and percentage different axle spacing error calculated in this research was 0.46 m and 8 % respectfully.
Generalized Method and Monitoring Technique for Shear-Strain-Based Bridge Weigh-in-Motion Comments: Measurement of shear forces closed to the bridge's support using Fiber optic Bragg granting rosette sensors. The Bridge size, type and stiffness of the bridges can affect the performance of the system	(Bao et al., 2016)	Maximum positive error in axle spacings 14.5 %, maximum negative error -11.9 %.
Novel virtual simply supported beam method Comments: Using measured strain signals from weighing sensors to estimate velocity and axle spacing	(He et al., 2017)	For 5-axle truck: Axle spacing maximum negative and positive error -5.9 % and 3.4 %, Velocity error -2.1 % and 3 %. For 3-axle truck: Max axle

directly. Identifies vehicle axles based on the flexural bending strains measured		spacing error -8.7 % and 4.6 %. Max velocity error -6.7 % and 3 %. For 2-axle truck: Max axle spacing error -3.4% and 4.3%. Max velocity error for that -2.5 % and 6.7 %.
Non-intrusive schemes for speed and axle identification in bridge-weigh-in-motion systems Comment: shear strain at the quarter points of span fails to identify axle numbers but accurately estimate the speed. However, shear strain at the beginning can detect both accurate axle numbers and speed.	(Kalhori et al., 2017)	Using flexural strain at mid and end span has speed calculation error no more than 4 % for 95 % runs. Shear strains at mid and three-quarter span had speed error less than 4 % and for 70 % run the speed error no more than 1 %.

This research proposed a novel method of using the geophone sensors for the first time as an axle detector in the BWIM systems to improve the accuracy of identifying local events significantly more than the existing methods. The truck velocity, the axle positions, and the axle spacings of the vehicles were estimated and validated experimentally with accurate results. The results estimated in this research significantly reduced the error achieved from the existing FAD systems and methods using the accelerometers. The experiments and results of this study will be explained in detail in the following chapters of the thesis.

3. Results and Discussion of Field Experiments

3.1 Introduction

Manitoba's highway network features ageing steel bridge structures subjected to increased axle loads, speed, and traffic intensity, all of which increase their degradation due to fatigue. Rapid replacement or restoration is impossible for old structures that have already reached the end of their useful life. A fatigue evaluation and damage assessment are used to determine the residual life of these sorts of structures or their components. Field measurements are reliable for determining fatigue loading. The city of Winnipeg is surrounded by the Perimeter Highway, which provides an alternate route around the city. Winnipeg is within an hour's drive from the US border. The city of Winnipeg has distribution capabilities due to its geographic importance, with routes flowing in all directions. The Trans-Canada Highway connects Victoria, British Columbia, to St. John's, Newfoundland. It is the world's longest national roadway, stretching 7,821 kilometres. Winnipeg has highly travelled truck traffic routes attributed to a network of interconnected motorways. The bridge-weighing-in-motion (BWIM) system monitors two bridges on the Perimeter Highway, one on each side.

The bridge at the northeast corner of the perimeter is known as PBY, while the bridge at the southern end is known as Winnipeg Bridge 1 (PBX). This research is on PBX. BWIM is chosen over commercially available pavement weighing-in-motion (WIM) systems because it is less expensive, requires less regular calibration, and causes minimal traffic disruption during installation. Although the WIM devices are precise, they are visible on the road, allowing the offending cars to avoid them. The BWIM systems, on the other hand, are non-intrusive and are

not visible above the bridge deck. Long-term SHM for bridges is being used in recent research projects to detect changes in the structural integrity of their fatigue-sensitive components. Fatigue life prediction for a steel bridge using BWIM data entails several sources of uncertainty.

The research's main objective is to increase the live load calculation portion of BWIM's accuracy by obtaining the precise locations of the axles and the axle spacings, which can then be combined and used to determine the individual axle weights of the heavy trucks that crossover the bridge.

3.2 Case Study: Winnipeg Bridge 1 (PBX)

The bridge shown in figure 3.1 is the Perimeter bridge, located in Winnipeg, Manitoba. This bridge is presently being observed by SIMTReC (the Centre for Structural Innovation and Monitoring Technologies). It has seven spans, four of which are continuous and three of which are simply supported which is supported by eight steel girders.

Fig 3.1. The South Perimeter Bridge

According to Fig 3.2. and Fig 3.3. the South perimeter bridge in Manitoba was instrumented with the geophone underside of the slab in span seven for conducting the proposed method using the geophone sensor. The geophone sensor was attached to the top of girder seven besides the bearing.

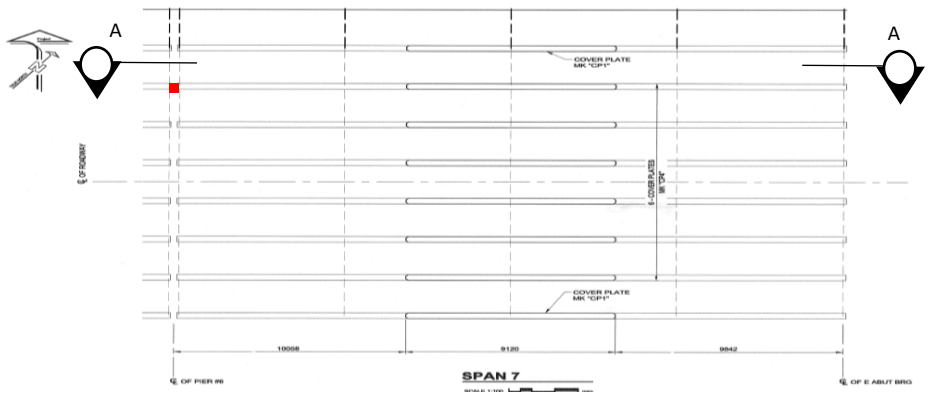

Fig 3.2. The plan of Span 7 and the position of Section AA.

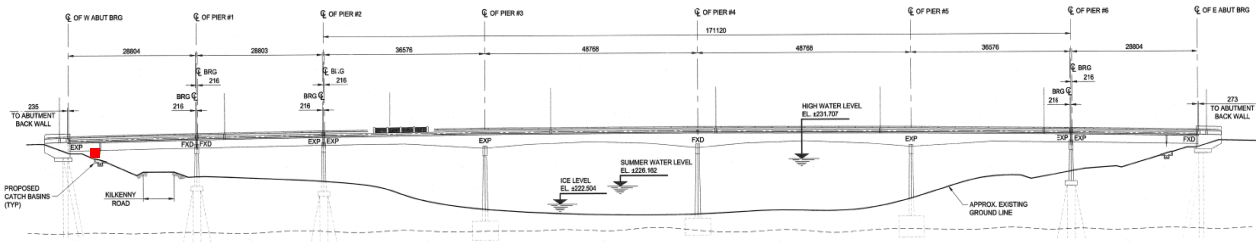

- Location of the geophone from the section AA

Section

Fig 3.3. The geophone's location in the section AA

The proposed method in the research uses the geophone to record the bridge's response to gather information on the truck configuration that crosses over the bridge. In this research, the bridge response is the bearing displacement caused by heavy truckloads across the bridge.

According to Fig 3.4. the experiment's primary objective was to estimate the axle spacings of the trucks using the geophone data. The axle spacing results are calculated with the geophone. Then the results will be combined with gross vehicle weights measured using the Strain Gauges and BWIM method (Faraz, 2020) to estimate the individual axle weight of the trucks in a future study.

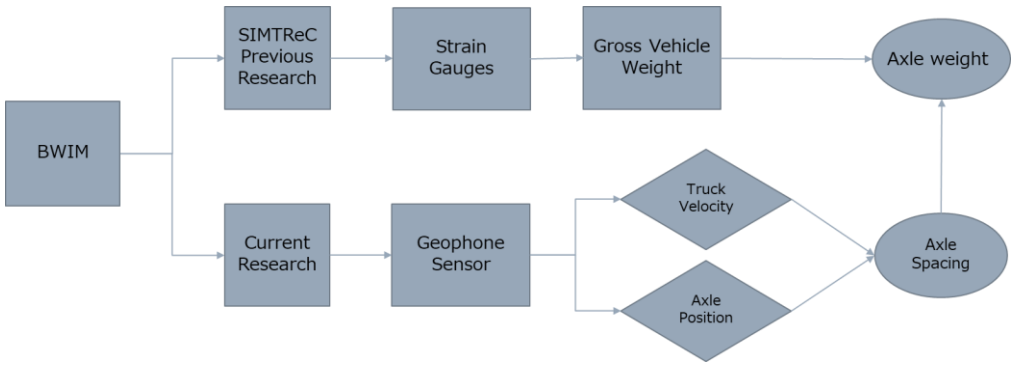

Fig 3.4. Shows the outcome of the BWIM system, which incorporates results from earlier, current, and upcoming research

The individual axle weights, as a result, offer comprehensive truck configuration data, which influences the computation of the live loads that the bridge will withstand over time to have more precise monitoring and prevent steels from fatigue during the lifetime of the structures. For this purpose, this research proposed using the geophone to collect data for calculating the velocity of the trucks, axle numbers and axle positions in the first part. Simultaneously the results were validated with the video camera attached above the bridge. Four distinct datasets of arbitrary heavy vehicles crossing the south perimeter bridge were collected for the velocity calculation and validation experiment for five minutes each. Then

based on the calculated velocity and the positions of axles from the first section, the following part was undertaken to estimate and validate truck axle spacings.

The next part will describe the activities conducted for experimenting with the proposed method in collecting data from the south perimeter bridge.

3.3 Field Test

As mentioned previously, the geophone was attached on girder seven besides the bearing in span seven which is shown later in Fig 3.9. The geophone used in this work, a model SG-5, has a natural cut-off frequency of 5 Hz and a sensitivity of 80 V/m/s, as shown in Fig 3.5.

Geophone Model	SG-5
Natural Cut-off Frequency (Hz)	5
Sensitivity (V/m/s)	80

Fig 3.5. Geophone information

Fig 3.6. This picture shows the end of the girder seven and the bearing to which the geophone was fastened. The geophone was supposed to record the bearing displacement as a vertical velocity of the bearing due to compression and bearing tension resulting from heavy truck loads crossing over span seven.

Fig 3.7. The place where the geophone was attached with putty on the girder seven under the second expansion joint

The geophone had been mounted on girder seven at the second expansion joint, resulting in low bridge dynamic response and extremely sharp peaks matching vehicle axles.

Fig 3.8. The geophone was attached to the teensy board with Arduino

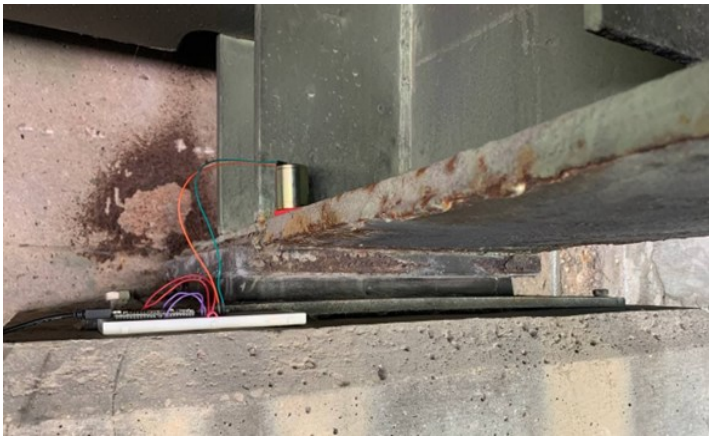

Fig 3.9. The geophone attached location and bearing from the side of view

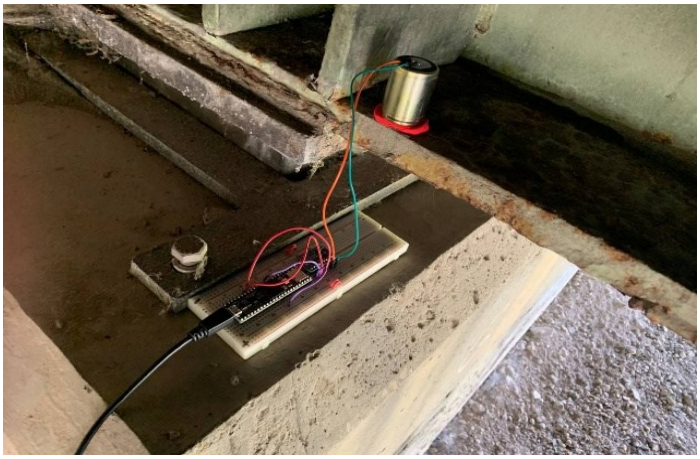

Fig 3.10. The teensy board with Arduino is connected to the laptop with a USB cable.

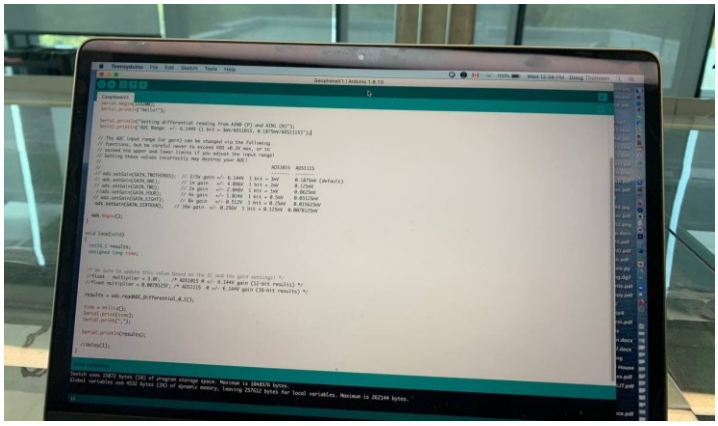

Fig 3.11. Data was received and extracted to a CSV file through Arduino software on a laptop.

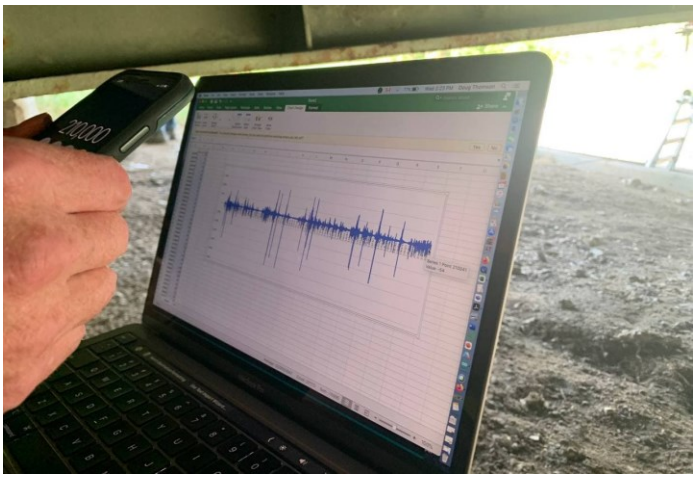

Fig 3.12. The first example of extracted excel file data received from the geophone for 5 minutes. The higher amplitude signals correspond to heavy trucks that travelled through a span of seven during the 5 minutes.

Four separate datasets were collected with this method. They were all received in 5 minutes duration and ready for analysis.

3.3.1 Converting Units from the Electrical Unit to the Mechanical Unit

Explaining the conversion of electrical units to mechanical units is worth mentioning in this part, which implies, in this case, converting voltage with the unit of volts (electrical unit) to velocity with the unit of meters per second (mechanical unit). The primary data received from the geophone were in bits. Each bit is equal to 0.015625mV. For example, a reading of 1450 bits is equal to 22.66 mV. The Geophone sensitivity is 80 V/m/s. Therefore, this would correspond to (0.022666 V) / (80 V/m/s) = 0.000283 m/s or .283 mm/s.

Following the conversion explanation, the voltage data's vertical axis was converted to the velocity unit. It is not the velocity of the truck in the longitudinal direction. It is the vertical velocity that causes by the compression (+) and tension (-) of the bearing that generates the vertical displacement. Due to the large volume of compression and tension caused by heavy and large-sized trucks, signals associated with heavy vehicles have higher amplitude in the vertical velocity versus time signal as the displacement increases due to larger weights and loads.

3.3.2 Separating and Filtering Signals with Longer Amplitude

The next step was separating the higher amplitude signals from the actual data and using the Python code to filter out all unnecessary noises. After filtering the separate heavy truck signals for each dataset, they were ready for analysis.

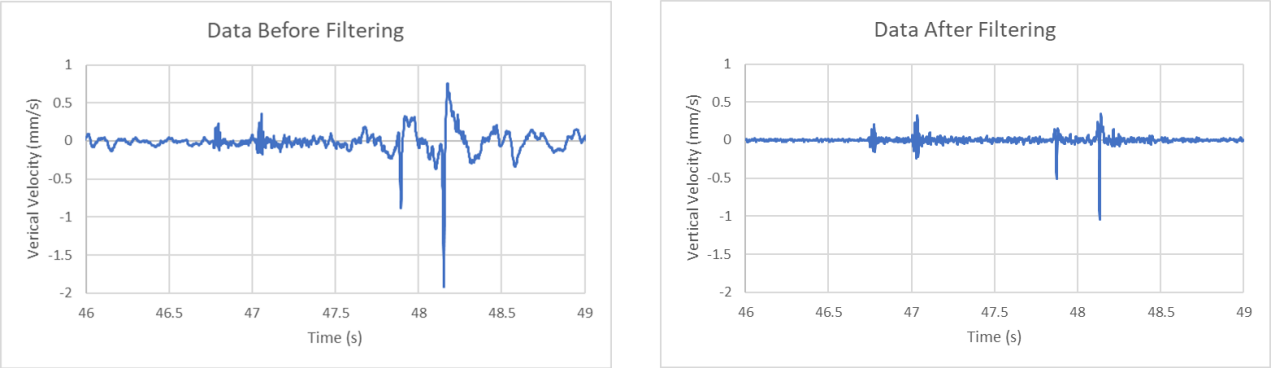

Fig 3.13. The example of the separated geophone signal for the specific truck with two axles before and after filtering.

3.3.3 Detecting the Configuration and Axle Numbers of Trucks

Based on the geophone signal example, the geophone recorded a series of positive and negative spikes in vertical velocity measurement. The spikes correspond to the bearing, which is compressed and released by each axle load when a truck passes. The configuration, numbers, and axle position can be estimated from the spikes in the signal, which are shown in Fig. (3-14). The sampling rate of the signals is equal to 100.

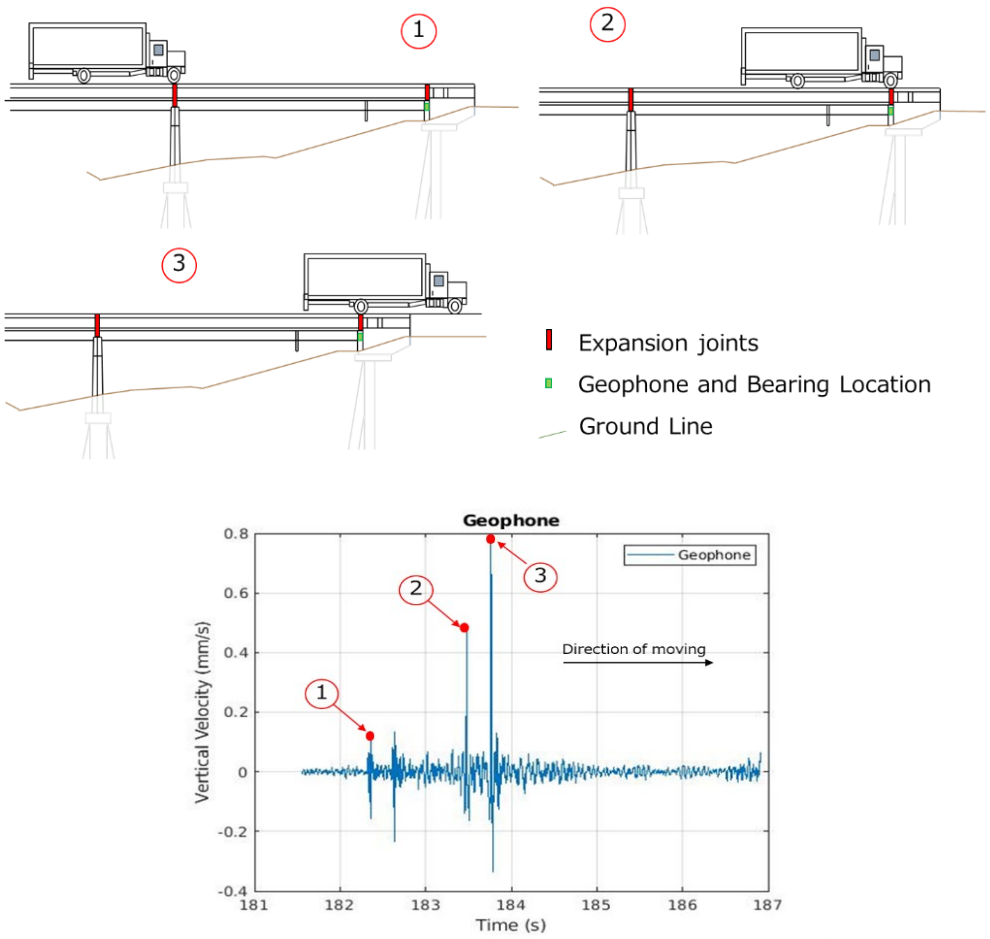

Fig 3.14. Represents the way of detecting the number of axles and axle positions when the trucks pass over the expansion joints based on the geophone signal

Fig 3.14. The bearing and the geophone location were determined underneath the second expansion joint. It was demonstrated that the geophone signal spikes were related to the vehicle's position and entry and exit timings from the span. At the same time as obtaining data from the geophone, the video camera was mounted above the bridge with a perspective of the first and second expansion joints of span seven. The objective was to verify the velocity results while observing the vehicles and their configuration while the geophone gathered the same information. Through the images from the video camera, one example of the position of

expansion joints is depicted in Fig 3.15. The pictures from the video camera also observed the axle numbers and the truck configuration.

Fig 3.15. The location of two expansion joints can be seen through the attached camera.

According to Fig 3.6. each signal received from the geophone for each truck has two sections. Section one (241 to 242 seconds), with a shorter amplitude, shows the positions when the axles enter the span, and section two (242 to 243 seconds), with a larger amplitude, represents the positions when the axles for the same truck leave the span. The geophone is located under the second joint, producing a larger signal for wheel loads over that joint. The timing of entering and exiting the span for the front axle based on this repetitive behaviour observed among all signals allows for calculating the truck's velocity.

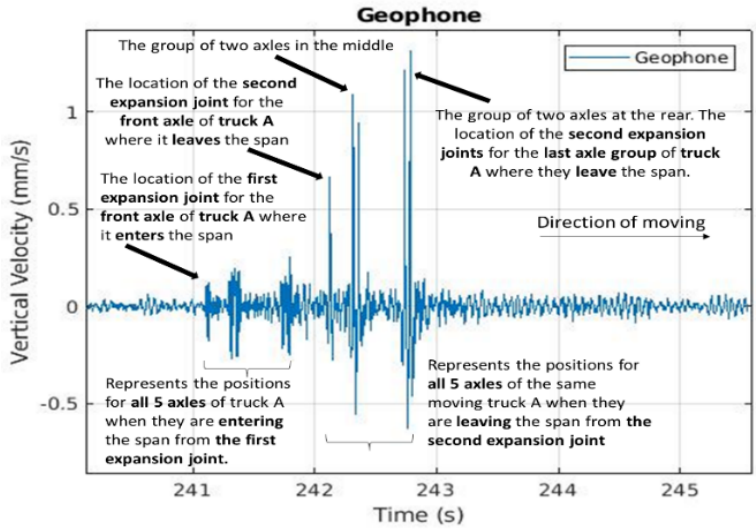

Fig 3.16. This signal represents one of the Geophone signals examples for a 5-axle vehicle entering and exiting the bridge. The identifying method to detect each spike was explained in detail. The geophone is situated under the second joint.

3.4 Estimating the Velocity of Trucks in the Field

3.4.1 Velocity Calculation Based on the Geophone Signals

Two different methods were used for the field test to estimate the velocity of more than 30 different trucks. The first method used geophone signals to calculate the velocity, and the second used video recordings to validate the results. The geophone velocity estimate used the time difference between the first axle entering and the first axle leaving the span. An example in Fig 3.17 is where the axle enters the span crossing the first expansion joint at 182.3s and crossing the second expansion joint, leaving the span at 183.5s. The velocity was calculated by dividing the distance between the expansion joints by the time difference.

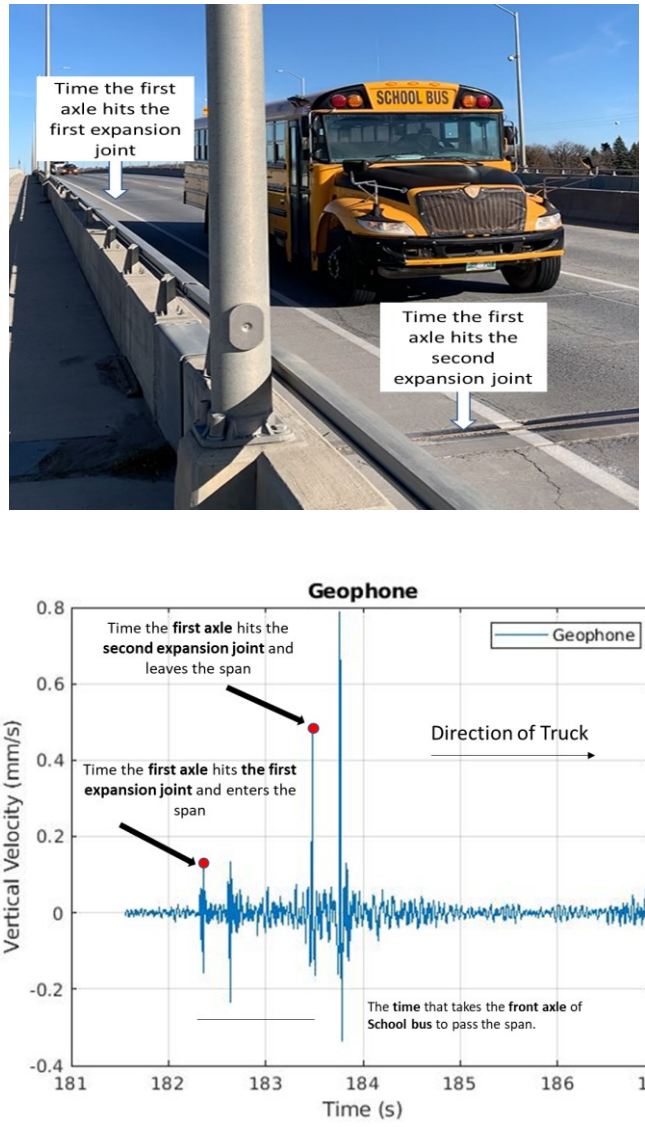

Fig 3.17. Detecting front axle positions and timing for velocity calculation

According to this method, the velocity, axle numbers and truck configuration for 35 trucks were calculated based on the signals received from the geophone.

3.4.2 Velocity Validation Based on the Video Camera

The other method of estimating the velocity is using video taken at the same time as the geophone recordings (Basheer Algohi et al., 2018). The starting time of the video and the geophone recording was synchronized for all four datasets. The video camera was set above the bridge to view the entering and leaving expansion joints on the Bridge Fig 3.18.

Fig 3.18. Represents the perspective and location of the video camera and the way of capturing the time that the front axle enters and exits the span. The second expansion joint is the location of the geophone.

The time between entering and leaving the front axle was determined by going through the video frame by frame. The velocity is calculated by subtracting entering and exiting times and dividing them by the span length.

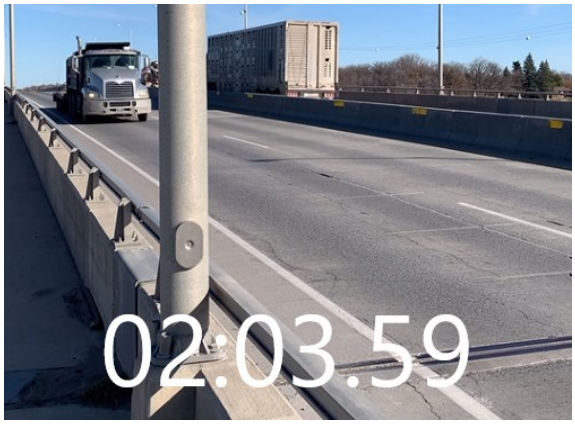

Fig 3.19. The entering time when the truck's front axle entered the span through the first expansion joint

Fig 3.20. The exiting time when the truck's front axle left the span from the second expansion joint

Based on the video analysis, the velocity of each truck was determined after considering the span length and the amount of time needed for the truck to cross the distance.

3.4.3 Velocity Results Comparison

Fig 3.21. The velocity result was estimated and validated for more than 35 trucks based on the geophone and video camera data. There might be differences based on the exact response

of the structures as the wheel enters and exits the span. However, the data estimation of the velocity base is represented here with a standard deviation equal to 4.6 % and a mean error equal to 1.9 %.

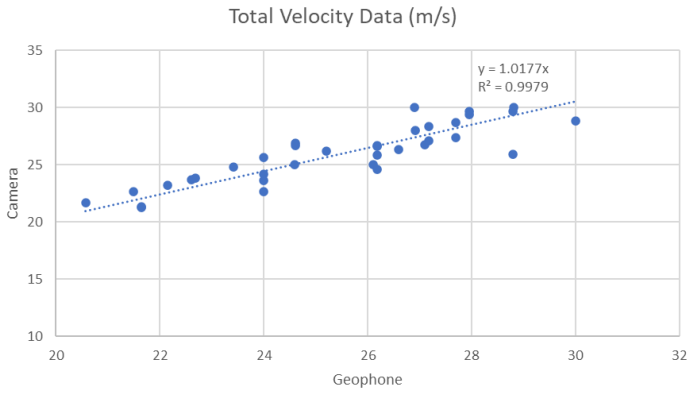

Fig 3.21. The total data velocity calculation of the camera versus the geophone

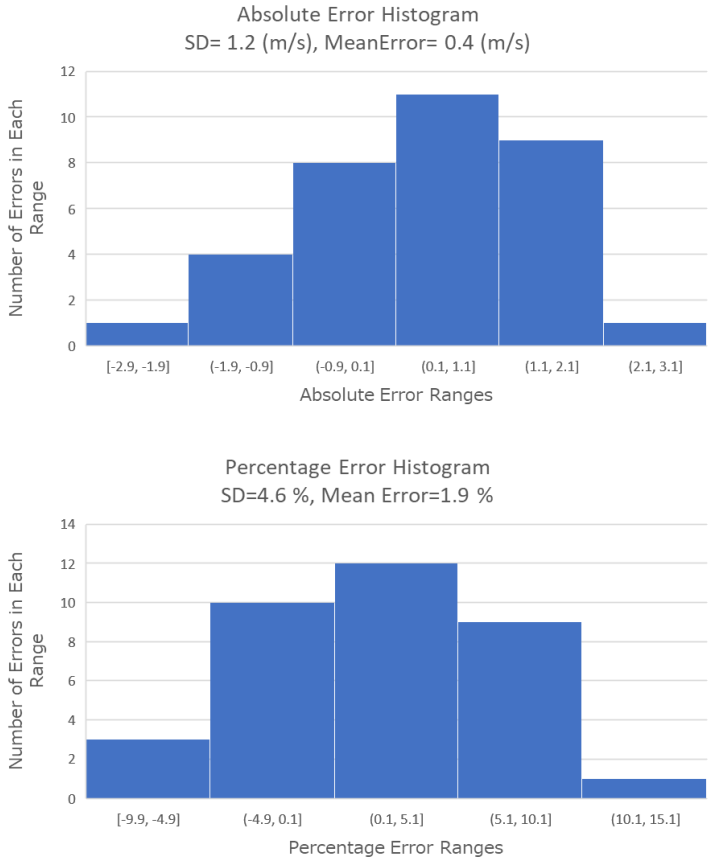

Fig 3.22. The absolute and percentage error histograms for total data velocity calculation

The trendline slope in total velocity data camera versus geophone equals 1.0177 based on Fig 3.21. According to the percentage error histogram, the velocity results are normally distributed with a 95 % Confidence interval between 0.42 and 3.48.

Table 3.1. The Summary of Comparison Velocity Results for Absolute and Percentage Error Histograms

Standard Deviation (m/s)	Mean Error (m/s)
1.2	0.47
Standard Deviation (%)	**Mean Error (%)**
4.6	1.9

3.5 Axle Spacings Calculation Based on Computed Velocity

When the velocity is known, the axle spacing can also be estimated. For this purpose, the other five distinct datasets, each lasting five minutes, were gathered. Fig 3.23. represents the geophone reattachment for calculating the axle spacing of heavy trucks.

Fig 3.23. The geophone position was attached to the top of the bearing for axle spacing calculations

Fig 3.24. The geophone was attached with the twisted cable to the laptop through the Analog Discovery 2

The next step involved separating the longer amplitude signals and changing the units from voltage to velocity, like the prior explanation. The signals were prepared for analysis after filtering. Fig 3.25. illustrates the procedures of calculation and validation of axle spacings using the geophone and video camera.

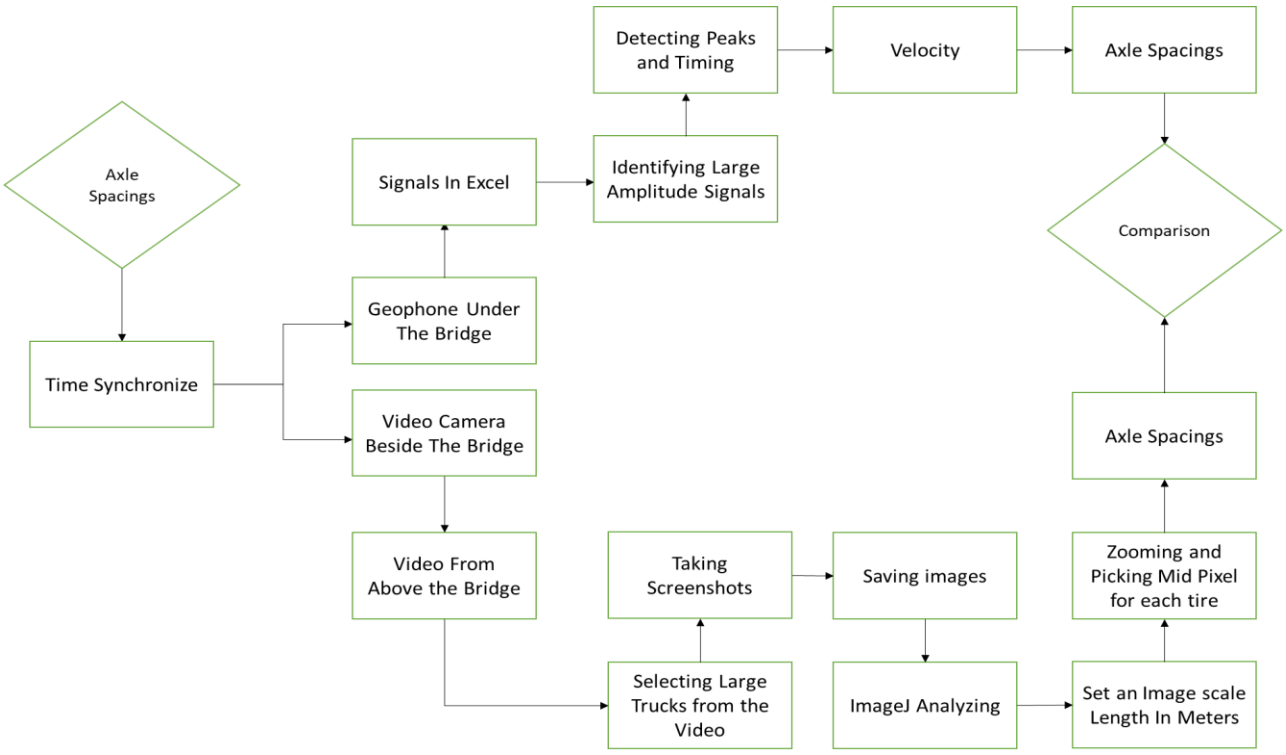

Fig 3.25. Shows the process of calculating and validating the truck axle spacings using the geophone and video camera.

According to Fig 3.25. two methods were used for calculating the axle spacings in this part. The first method used the geophone signals, and the second method used the camera with the perspective parallel to trucks beside the bridge to validate the axle spacing results received from the geophone. The time was synchronized between the geophone and the video camera while receiving data.

3.5.1 Axle Spacing Calculation Based on the Geophone Signals

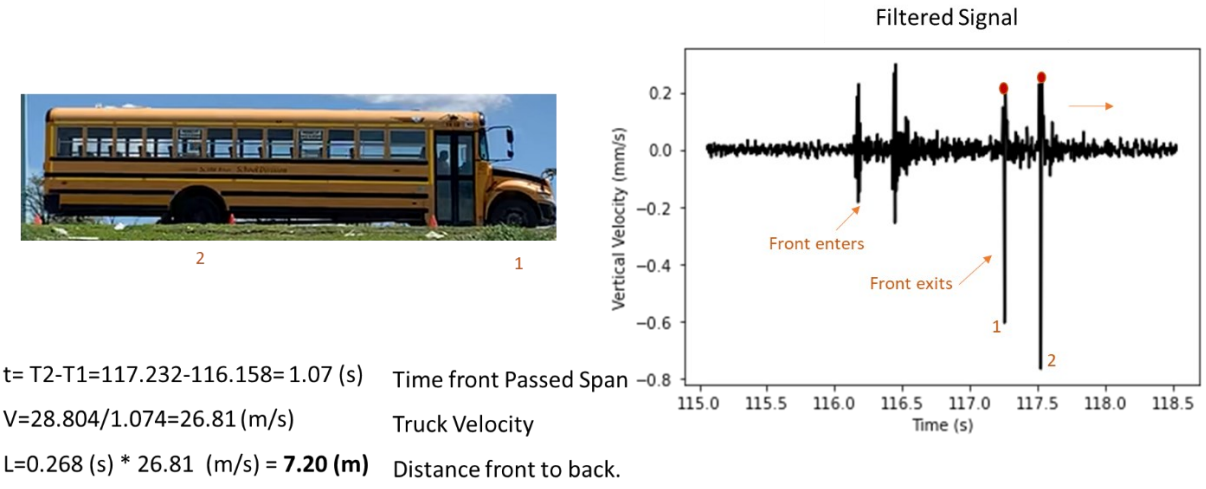

Fig 3.26. Illustrates the way of calculating the axle spacings based on the geophone signals for one example truck.

The velocity was calculated for all heavy trucks based on the previous explanation. This time, the second section of the signals related to the location of the second expansion joint when the axle leaves the span is considered for determining axle spacings.

The time when each axle leaves, the span can be determined based on the geophone signals. An example is shown in Fig 3.27. for a 5-axle truck. Each axle is marked with a red dot. The distance between each axle can be calculated by knowing the time for each point and the velocity. The results were then compared with video estimates using the above methods for velocity estimation.

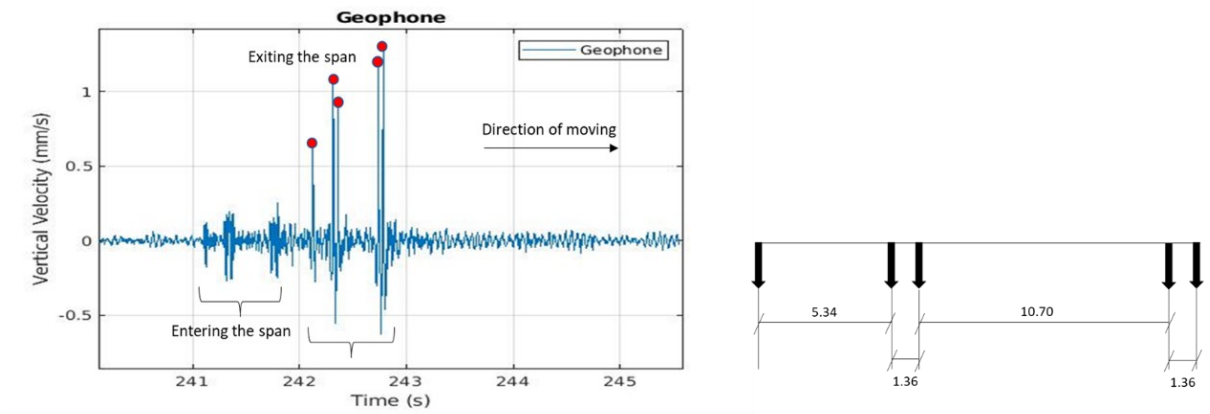

Fig 3.27. Calculated configuration of the 5-axle truck event. Peaks determine the number of detected axles exiting the span.

3.5.2 Axle Spacing Validation Based on the Image Analysis

3.5.2.1 Setting the Place of the Video Camera

For verification of the calculated results based on the geophone data, at the same time as receiving data from the geophone, the video camera parallel to the bridge was attached with the known distance and angle from the first wheel line of the trucks, as shown in Fig 3.28.

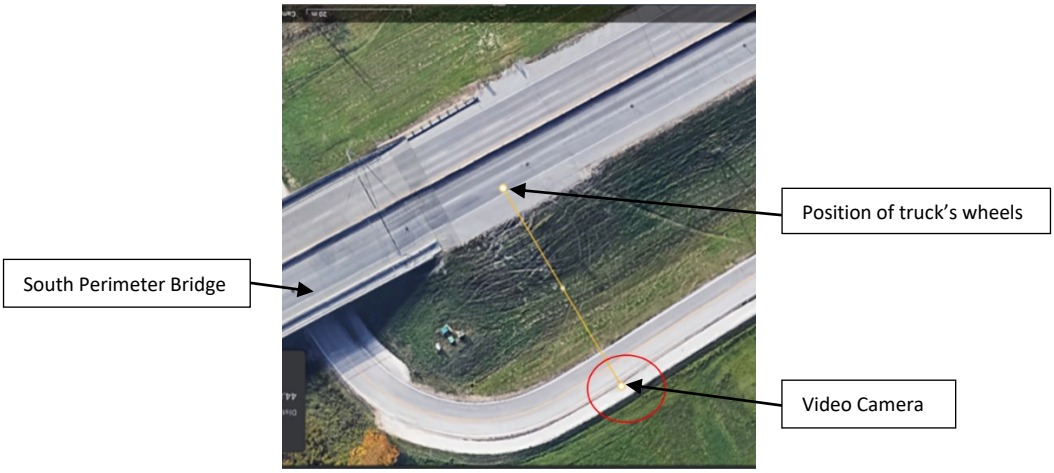

Fig 3.28. Position of the camera from the first lane of the highway on google earth

Fig 3.29. Position of the camera from the different perspective

Fig 3.30. The Left Picture is a picture of the bridge from the camera's perspective. The Right Picture is a Screenshot frame from the video used in the analysis to be able to observe the truck wheels.

3.5.2.2 Setting the Known Scale Distance in the Fixed Frame of Screenshots

After adjusting the location of the video camera and determining the screenshot frames, three cones spaced 4 metres apart (total 8 meters) were used to represent the known length

space in each video frame. Throughout all five datasets, the scales and camera placement remained the same.

Fig 3.31. An example of a video frame with cones as a known-length scale.

3.5.2.3 Analyzing the Screenshots Received from the Video Camera

After obtaining five videos for five datasets, screenshots were taken from the large vehicles in the videos. The time of the screenshots was then verified to find the relative signals using the geophone signals separately. Images were analyzed after being compared to the relevant signals in the screenshots. Fig 3.32. illustrates the proper procedure for image analysis in this section.

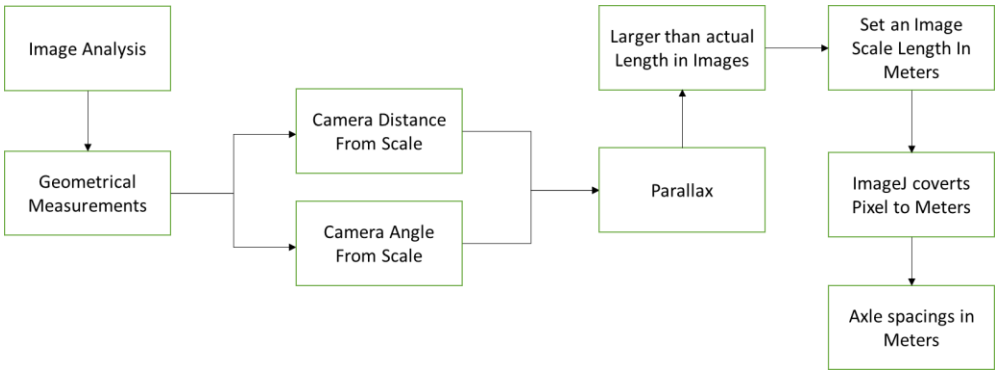

Fig 3.32. Shows the process of image analysis for calculating truck axle spacings

The first significant aspect of the image analysis was the consideration of the geometrical measurements, which directly impacted the computation process. According to Fig 3.33. due to parallax caused by the distance and angle of the video camera from the truck's wheels, the actual length, which was 4-meter would be 11.5 % (5.2/45) longer in the pictures. Based on the explanation in the image analysis, the length of the scale was considered as 4.5 meters. It is important to note that due to the variation in the wheel position in the wheel path, there might be +/- 0.6% uncertainty in the analysis here.

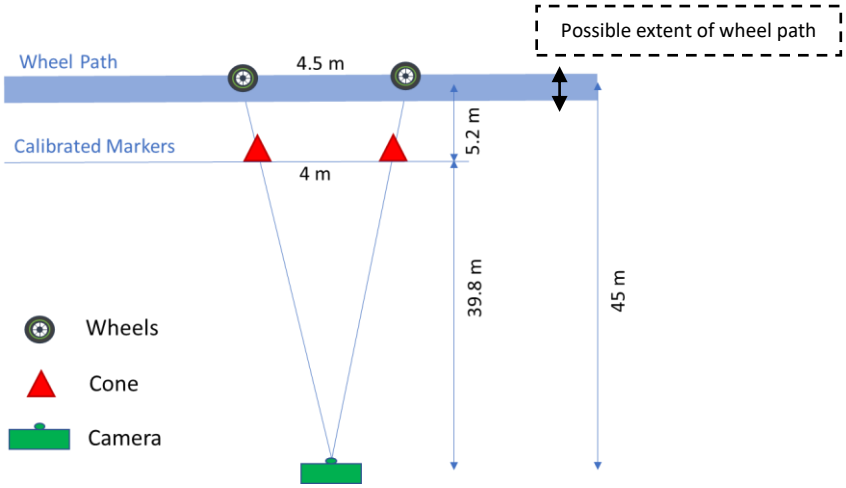

Fig 3.33. Geometrical Measurement Explanation

3.5.2.4 Axle Spacing Calculations in ImageJ Software:

For image processing, the software called "ImageJ" was used. The software environment is depicted in Figure 3.34.

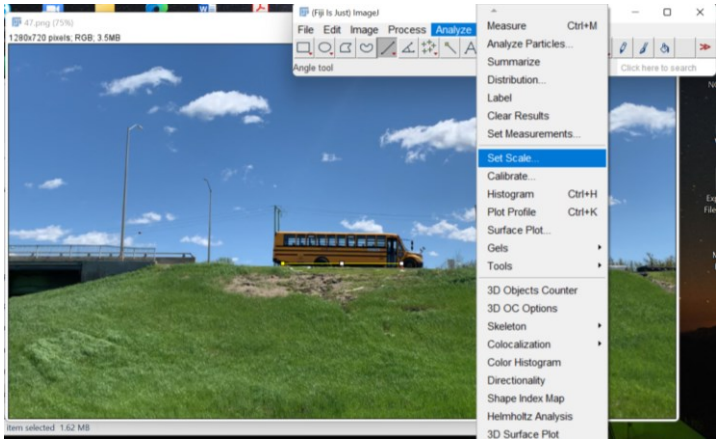

Fig 3.34. ImageJ Software Environment

The first step was setting the known scale length by considering the geometrical measurement in the program. The ImageJ software used the known scale length in meters and converted the pixel length into meter length. The length of the cones' mid-pixels was detected and introduced as a known length in metres for setting. After setting the scale by zooming the picture and identifying the mid pixels of each tire in the trucks, the axle spacings were calculated.

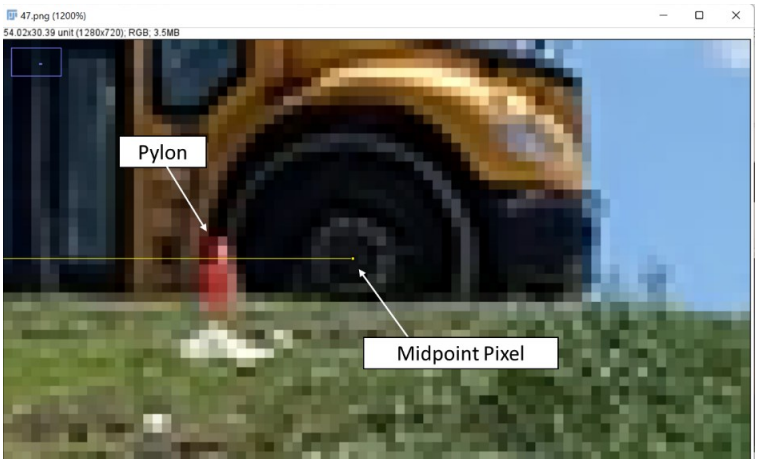

Fig 3.35. The mid-pixel of the tires was identified by zooming the picture and using the available software tools.

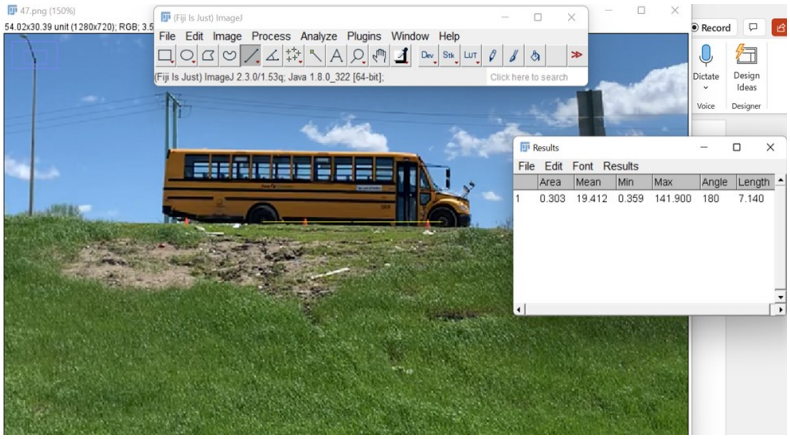

Fig 3.36. This picture shows the mid-pixel distance between two school bus tires is 7.14 meters.

This procedure was repeated for five random trucks with three axles using three multiple frames to examine the reliability of the axle spacings computation based on this methodology. Fig (3-37) represents the example of the result for one truck in multiple screenshots.

Axle Number	Frame 1 (m)	Frame 2 (m)	Frame 3 (m)
1-2	4.60	4.62	4.63
1-3	6.10	6.13	6.15

Fig 3.37. The axle spacing results based on this image processing show one truck in multiple different frames

According to Fig 3.37. the estimated axle spacing answers were almost the same for all three frames for five trucks, which illustrates the method's reliability in this part. The results are shown in Table 3.2. for all five trucks.

Table 3.2. The Summary of Axle Spacing Results for the Five Trucks in the Different Frames

Truck	Axle Number	Frame 1 (m)	Frame 2 (m)	Frame 3 (m)
Truck 1	1-2	4.64	4.65	4.70
	1-3	6.00	6.03	6.11
Truck 2	1-2	4.60	4.62	4.63
	1-3	6.10	6.13	6.15
Truck 3	1-2	5.05	5.07	5.11
	1-3	6.35	6.37	6.43
Truck 4	1-2	4.03	4.05	4.08
	1-3	5.42	5.42	5.48
Truck 5	1-2	5.83	5.89	5.97
	1-3	7.21	7.29	7.35

Four random trucks were selected to check the other uncertainties, such as optical distortion, when using the camera to estimate velocity and axle spacing. For each truck, five frames were picked near the centre of the image. The axle spacing between the front and second wheel was calculated for those five frames relative to the distance from the front wheel to the central pylon. Fig 3.38. shows the axle spacing calculation versus the distance between the front wheel to the central pylon and the area where the measurements were usually done in each frame for four trucks. It represents that in bounds of measurements, for every 3 meters, there is a maximum 0.06 (m) difference in axle spacing results for each truck due to optical distortion, which made a maximum error equal to +-1%.

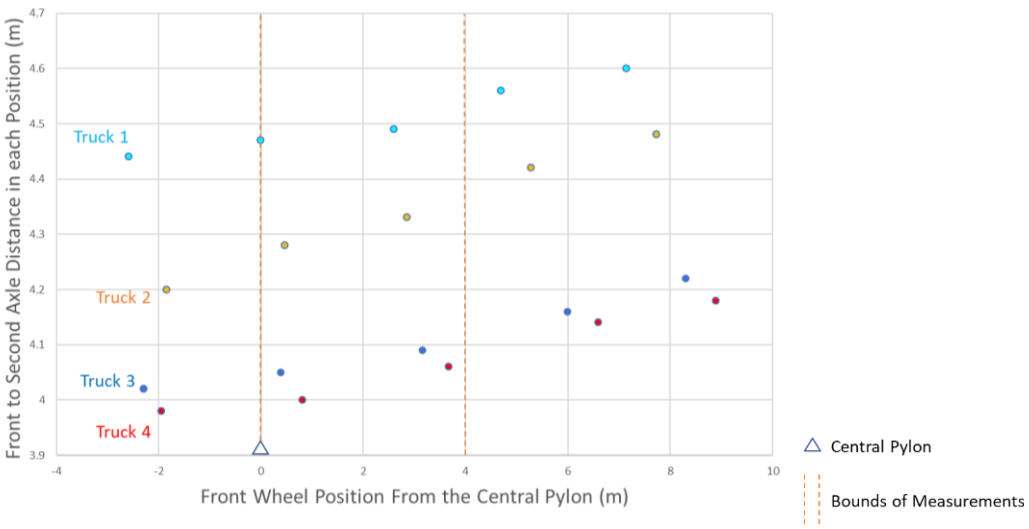

Fig 3.38. Represents the front-to-second axle distance in each frame versus the position of the front wheel to the central Pylon for four different trucks in five different frames

3.5.3 Axle Spacing Results Comparison

Over 50 trucks' axle spacings were calculated using this method. The graphs below compare geophone and video camera data for more than 51 trucks. For this comparison, three separate data orders were sorted. The first order includes all front group axles (data longer than 5 metres), the second contains data from all pair wheel groups (data less than 2 metres), and the final list has the total data. The trendline slope in geophone versus camera result graphs for all three data orders is almost 1. From the three percent error histograms, the axle spacing results seem normally distributed, and the 95 % Confidence interval level is considered in the data analysis. It is worth mentioning that because the video analysis was done frame-by-frame, there would be a + - 3 % uncertainty in this analysis.

3.5.3.1. Result Comparison of the Geophone Axle Spacing with the Video Axle Spacing for Front Group Data:

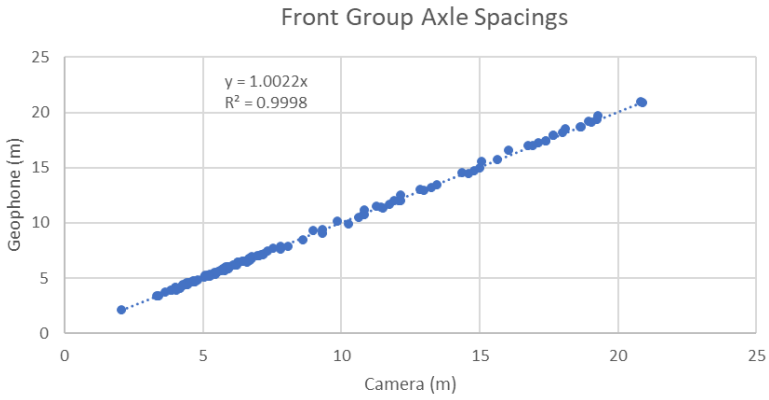

Fig 3.39. Front group axle spacing (Less than 5 meters) estimation for 51 trucks geophone versus camera with the trendline slope close to 1.

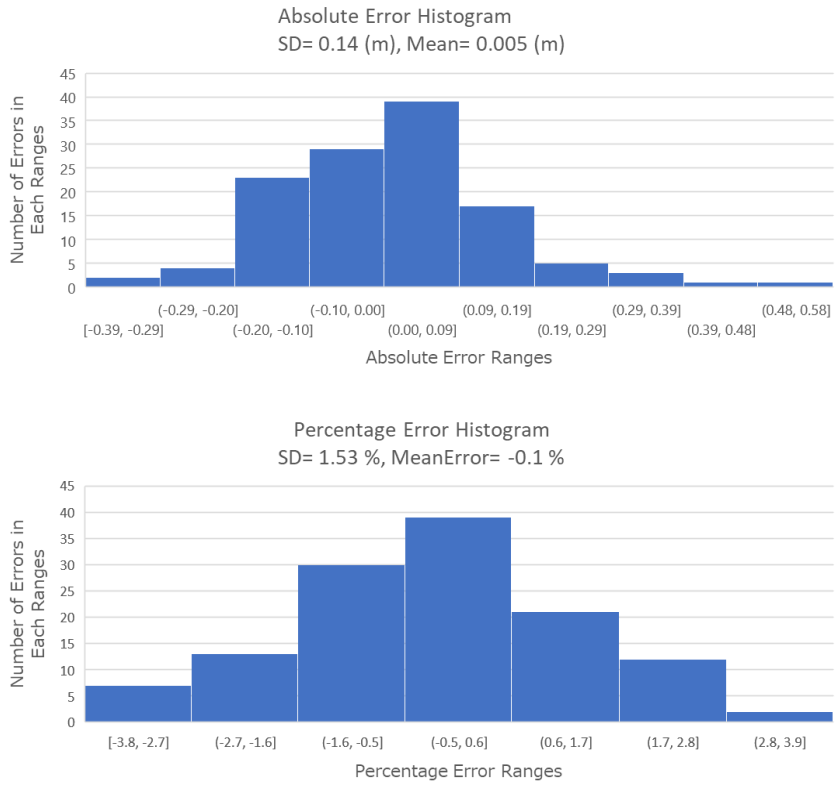

Fig 3.40. The absolute and percentage error histograms for the front group axles

The trendline slope of the front group axle spacings data, geophone versus camera, equals 1.0022, according to Fig 3.38. According to the percentage error histogram, the velocity results are normally distributed with a 95 % Confidence interval between -0.37 and -0.16.

Table 3.3. The Summary of Front Groups Axle Spacing Percentage and Absolute Comparison Results

Standard Deviation (m)	Mean Error (m)
0.14	0.005
Standard Deviation (%)	**Mean Error (%)**
1.53	-0.10

3.5.3.2. Result Comparison of the Geophone Axle Spacing with the Video Axle Spacing for the Group Data with Shorter Length

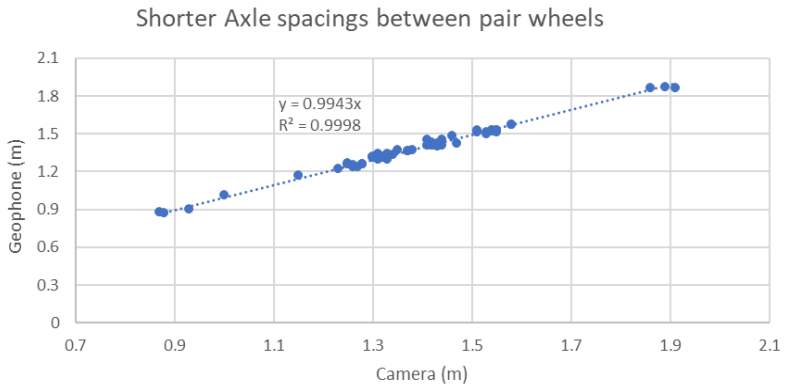

Fig 3.41. Pair wheels (Less than 2 meters) axle spacing estimation for 51 trucks geophone versus camera with the trendline slope close to 1.

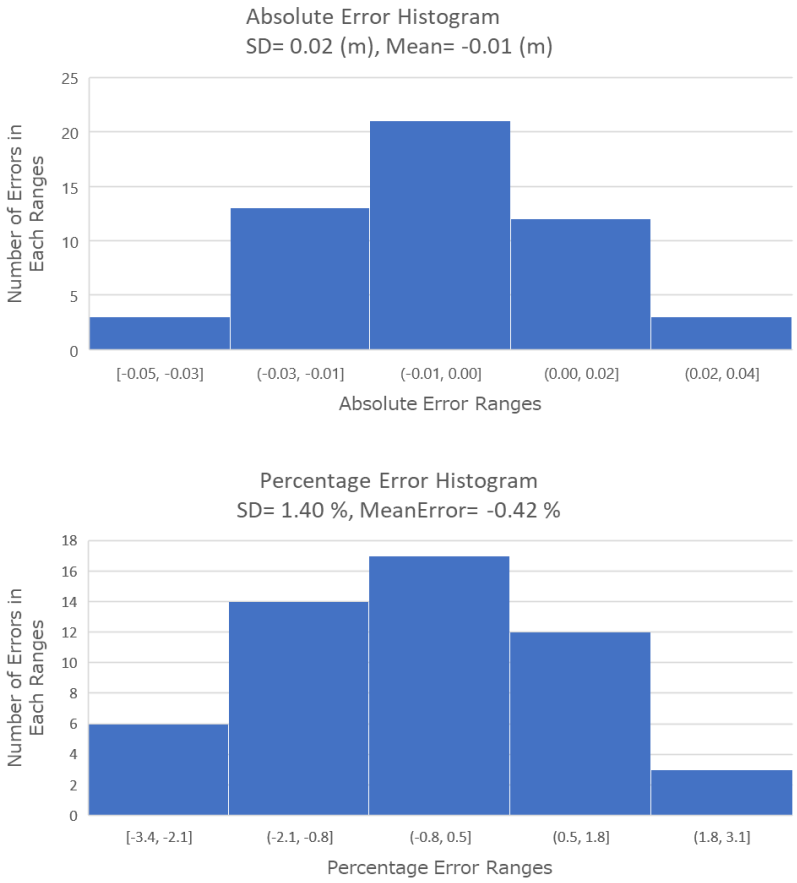

Fig 3.42. The absolute and percentage error histograms for the pair wheels group axles

The trendline slope in shorter axle spacing between pair wheel geophone versus camera equals 0.9943. According to the percentage error histogram, the velocity results are normally distributed with a 95 % Confidence interval between -0.80 and -0.05.

Table 3.4. The Summary of Axle Spacing Comparison Results for the Less than Two Meters Distances

Standard Deviation (m)	Mean Error (m)
0.02	-0.01
Standard Deviation (%)	**Mean Error (%)**
1.4	-0.42

3.5.3.3. Result Comparison of the Geophone Axle Spacing with the Video Axle Spacing for Total Data

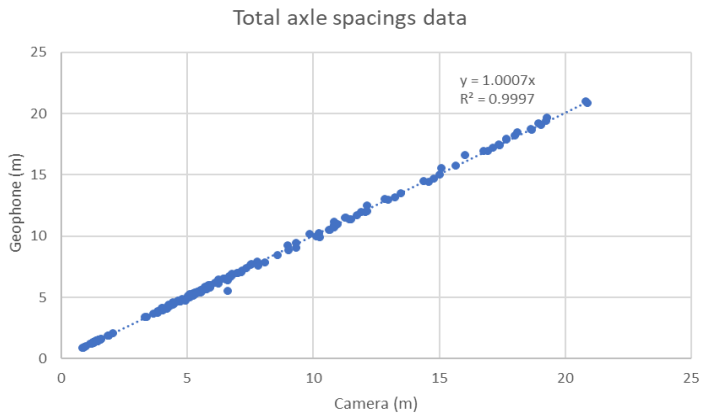

Fig 3.43. Total axle spacings data for 51 trucks geophone versus camera with the trendline slope close to 1.

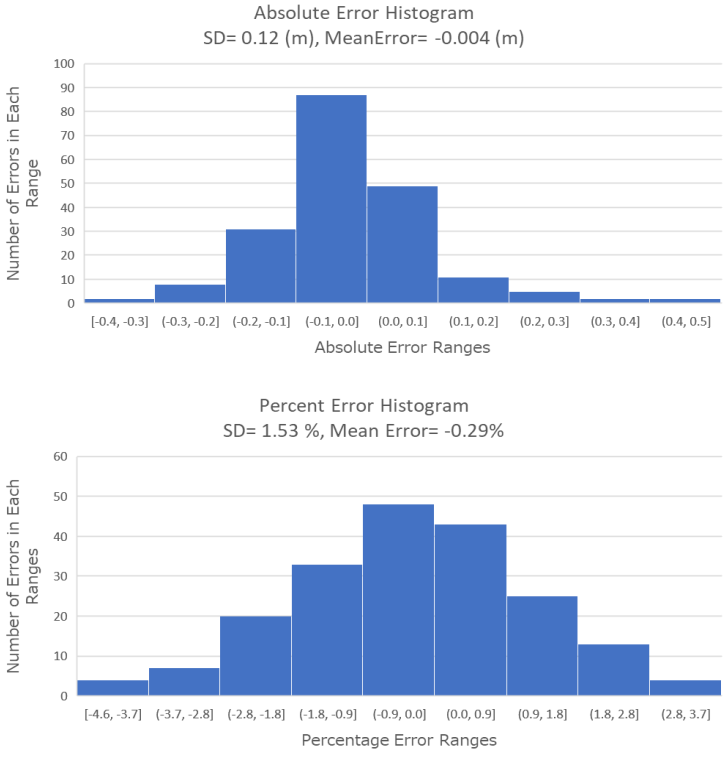

Fig 3.44. The absolute and percentage error histograms for the total group axles

The trendline slope of total axle spacing data, geophone versus camera, equals 1.0007. According to the percentage error histogram, the velocity results are normally distributed with a 95 % Confidence interval between -0.50 and -0.08.

Table 3.5. The Summary of Total Axle Spacing Results for Absolute and Percentage Error Histograms

Standard Deviation (m)	Mean Error (m)
0.12	-0.004
Standard Deviation (%)	**Mean Error (%)**
1.5	-0.2

3.6 Second Method of Velocity Calculation Using Side View

The final step involved revalidating velocity using the camera position from the previous section. The side view from the camera was used to determine the velocity of 45 trucks in this part. Fig 3.44. is shown as the procedure of estimating the velocity using this method. According to the flow chart, the first step was finding the two frames associated with when the truck's front axle was so close to the first pylon cone and when the front axle was near the third pylon cone. Based on the video camera, per second has 30 frames. The time the truck's front axle needed to pass the first and third pylon cones was calculated with video analysis by counting the frames between two designated frames. After calculating the time, the distances of the front wheel to the pylon cones for two defined frames were calculated in the ImageJ software.

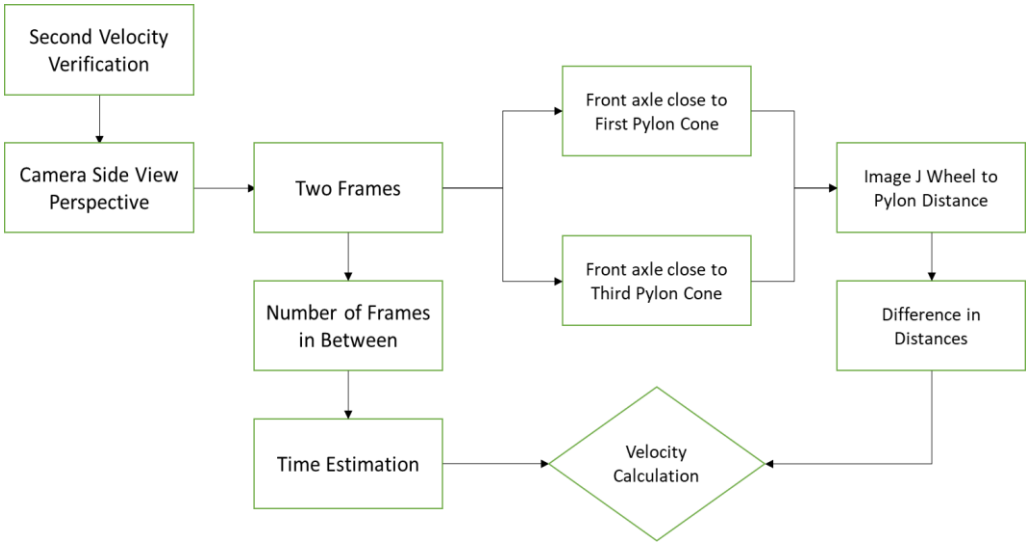

Fig 3.45. Represents the procedure of calculating the velocity for the second time from the side view.

3.6.1 Image Analysis and Second Method Velocity Verification

The figures below represent the two designated frames. Fig 3.45. The truck's front axle was closest to the first pylon cone, which shows the location. Fig 3.46. Twelve frames later, the truck's front axle was nearest to the third pylon cone.

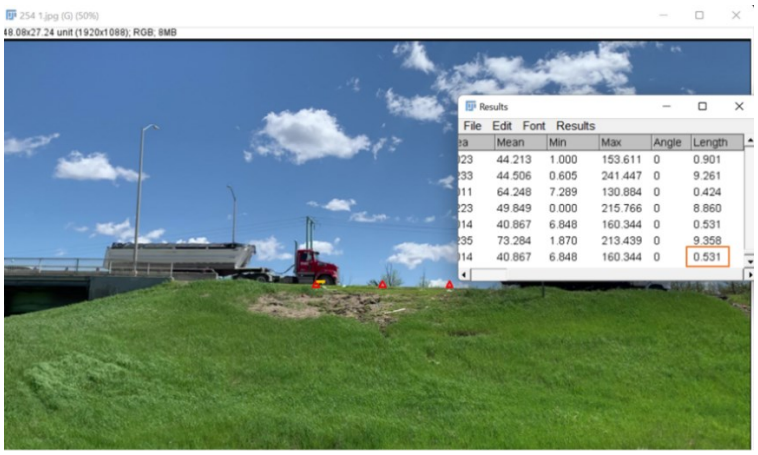

X1

Fig 3.46. Displays the measured distance from the first wheel to the first pylon cone that was calculated as X1 through ImageJ software

X2

Fig 3.47. Represents the estimated distance from the first wheel to the first pylon cone that was calculated as X2 through ImageJ software

As previously stated, the truck travelled from Fig 3.45. to Fig 3.46. in 12 frames. As a result, the time it took for the truck to pass was 12/30 (30 frames per second), or 0.4. (s). The distance was also determined using the distances from the front wheel to the first pylon cone in the two designated frames, Fig 3.45. and Fig 3.46. The truck's velocity calculated in this example was 22.05 m/s. The result was then compared with the geophone velocity, which was 22.3 m/s in this case.

The image analysis was done for all 45 trucks, and the results were compared with the geophone velocity calculation, as illustrated in the following section. It is worth mentioning that because the video analysis was done frame-by-frame, there would be a + - 3 % uncertainty in this analysis.

3.6.2 Second Method of Velocity Results Comparison from the Side View

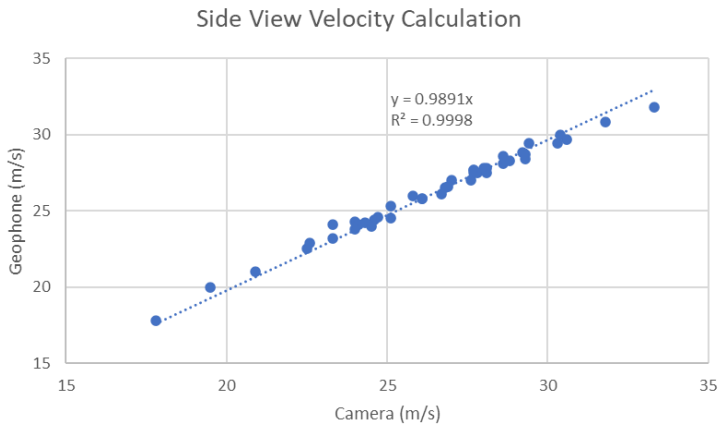

Fig 3.48. Second method of velocity calculation data geophone versus camera with the trendline slope close to 1 for 45 trucks

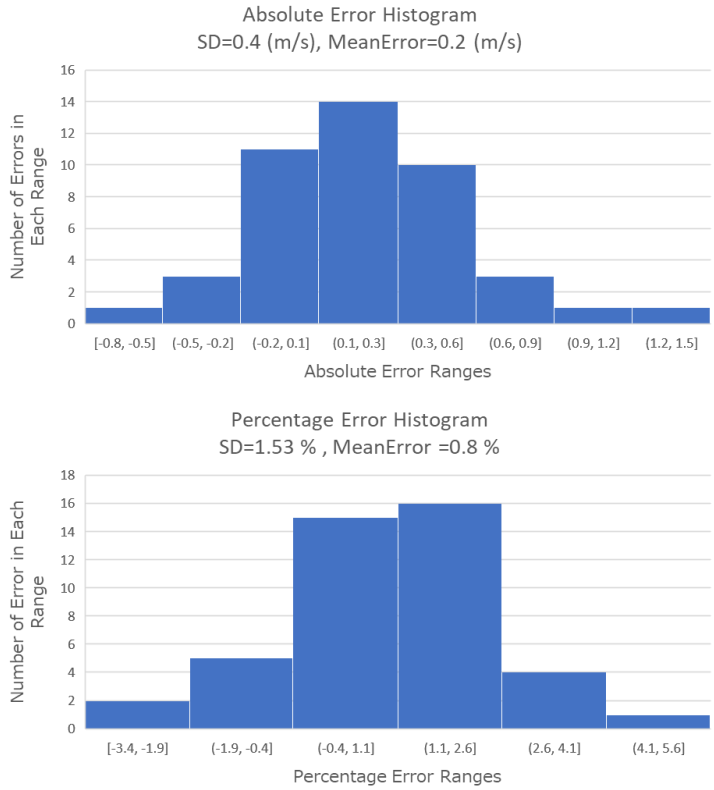

Fig 3.49. The absolute and percentage error histograms

The trendline slope in total velocity data geophone versus camera equals 0.9891. According to the percentage error histogram, the velocity results are normally distributed with a 95 % Confidence interval between 0.39 and 1.29.

Table 3.6. The Summary of Second Method Velocity Comparison Results for Absolute and Percentage Histograms

Standard Deviation (m/s)	Mean Error (m/s)
0.4	0.26
Standard Deviation (%)	**Mean Error (%)**
1.5	0.8

Due to the camera's parallel location and the system's different setup in this section, the error percentage in the second technique of velocity validation was reduced from 1.95% to 0.8%, with a standard deviation of 4.68% to 1.53%. As a result of explained experiments on the actual bridge, the geophone accurately determines the truck's velocity and axle spacing with reasonable accuracy. So, the geophone can be used as an axle detector which then could be incorporated into a BWIM system.

This technique is also applicable to shorter-span bridges for long-length trucks. It is possible that overlapping occurs due to the truck length exceeding the span length between truck wheels entering and truck wheels leaving that have the information of the first and second expansion joints. This issue can be solved by using two geophones under each expansion joint to detect the information of each expansion joint separately for calculating the axle spacing of the truck that has a length greater than the length of the span. The first and

second expansion joints' axle positions can be precisely determined from the data received from the two Geophones.

3.7. Error Analysis

The Table below summarizes some uncertainties that might happen during the field experiments, which might affect the trucks' measurements of the velocity and axle spacings.

Table 3.7. Method Uncertainties

Source	Comments	Error
Quantization Error as Frame-by-Frame Video Analysis (Using the video frame as an actual time)	Video Has 30 Frames per Second	+- 1.5 %
Quantization Error in the Geophone (Using the geophone as an actual time as well as in the part of manual measurements)	Geophone Sampling Rate 1000 per Second	+- 0.05 %
Frame Reproducibility (In the part of manual measurements)	20 Times Calculation for the Same Frame	+- 0.4 %
Optical Distortion Error (In the part of manual measurements)	Front to Second Axle Spacing Calculation in 5 Different Frames. For 3 Meters, Maximum 0.06 Difference.	+- 1 %

The first method using frame count to estimate velocity, has errors due to video quantization and geophone quantization. Therefore, the total error is expected to be 1.5 + 0.05 or +-1.55%. The frame-to-frame position difference method of velocity estimate has errors due to geophone quantization, operator reproducibility, and optical distortion. In this case, the total error is estimated to be 0.05%+0.4%+1.5% for a total of +-1.95%.

4. Results and Discussion of Laboratory Experiments

4.1 Introduction

Laboratory experiments in this research were done in the structural health monitoring laboratory at the University of Manitoba. The same geophone methodology was duplicated using a model bridge in the laboratory to explore further and clarify the geophone method for estimating the velocity and axle spacing. The model bridge has structural characteristics scaled to the bridge used for field experiments. This small-scale bridge model was chosen to evaluate the issues associated with BWIM systems. The model was built by (Sofia Faraz et al. 2020) based on a south perimeter bridge in Winnipeg, Manitoba. The assumption was that the model research would validate BWIM readings and aid in assessing a bridge's fatigue response. It is an elastic model that is expected to be capable of obtaining influence diagrams. Although this is geometrically like the prototype, it is made of a homogeneous, elastic material separate from the material used in the prototype. In this study, the model bridge was equipped with a geophone to calculate the velocity and axle spacings of the model truck that travelled over the model bridge.

4.2 Scaled Model Bridge

A bridge structure of a smaller scale was created utilizing a scale reduction of approximately 1:10 (Sofia Faraz et al., 2020). The scaled bridge was made of polycarbonate. Acceleration and deceleration ramps are on either side of the bridge's central main span. All three segments have a 3-meter span, as shown in Fig 4.1. The model bridge has four girders, as

shown in Fig 4.4. The model was instrumented with a geophone under the main span in the middle, on girder two, for the velocity and axle spacing estimation.

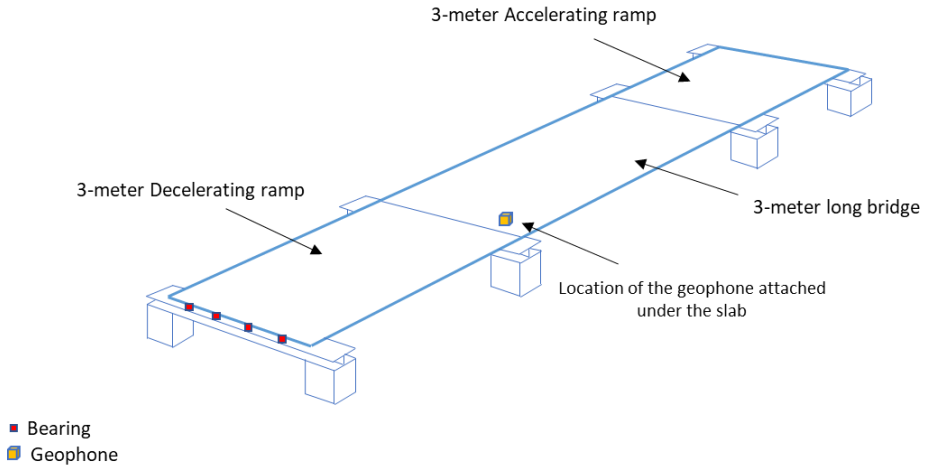

Fig 4.1. South Perimeter bridge small-scale model and the location of the geophone attached under the expansion joint

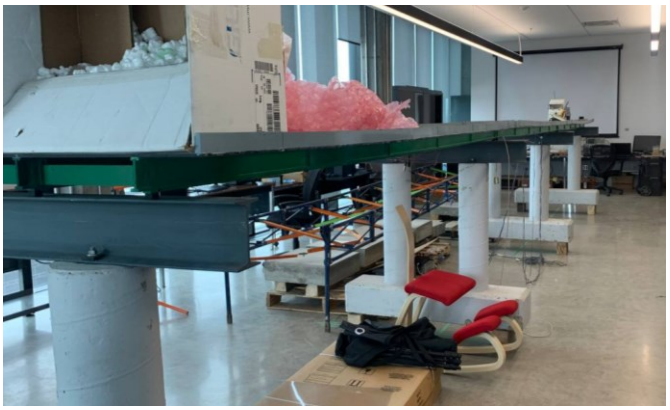

Fig 4.2. South Perimeter bridge small-scale model in the SHM laboratory

Fig 4.3. 3-meter span in the middle.

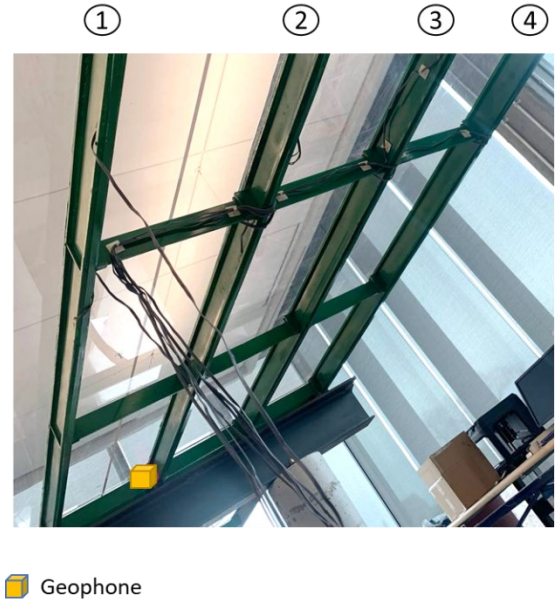

Fig 4.4. Represents the underside of the middle span of the model bridge, which has four girders, and the geophone was attached to girder number two

Regarding the mechanical properties of the model scale in the laboratory, Lexan was used for the model's manufacturing due to its low modulus of elasticity. Lexan produces large deformations even under light loads. The thermoplastic polycarbonate sheet (Lexan 9034), which is lightweight, easily machined, easily cemented, and quickly built, was used in this

model. The girder section's sectional characteristics are created to close the gap between the natural frequency and the prototype bridge. Girders are attached to the slab with glue in the bridge model. The model bridge's deck is also supported by 19 mm x 19 mm x 12.3 mm soft neoprene pads as firm bridge bearings, which provide good flexibility. For the ratio of the model truck to the model bridge frequency to be the same as that of a truck travelling at 100 km/hr on an actual bridge, the model vehicle's velocity should be computed (Sofia Faraz et al., 2020).

The Strain gauges at three transverse sections of the centre span for all girders were used as measuring devices for the prior experiment on the model bridge. They were installed at the bottom of each girder web at three transverse places on the model for estimating the gross vehicle weight in the BWIM system.

4.2.1 Data collection system

In this research, the geophone was fixed to girder number two with putty and connected to the laptop via a teensy board, as illustrated in Fig 4.5.

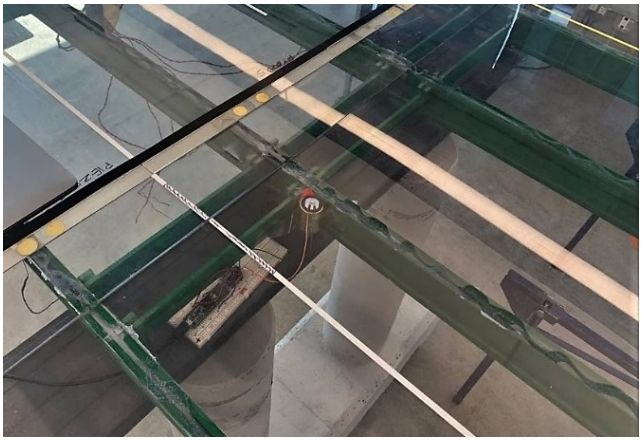

Fig 4.5. The location of the attached geophone to girder two from the top perspective

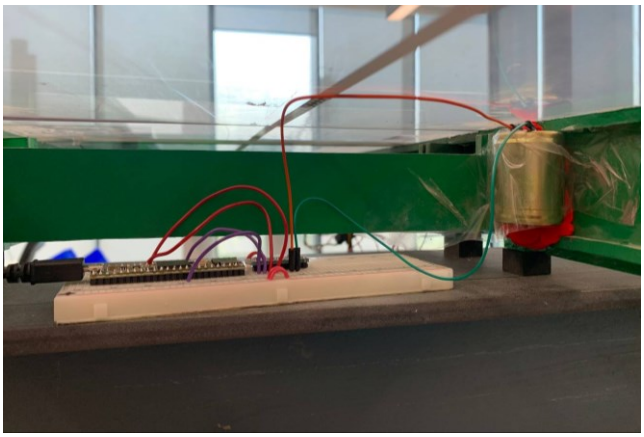

Fig 4.6. The way of initially fixing the geophone to the girder and teensy board with a USB cable

The primary method of collecting data in the lab was using a teensy board and Arduino software to collect and convert data to excel files, as shown in Fig 4.6. The second data collection method involved gathering data from the geophone and the strain gauges simultaneously using the multi-sensor measurement device to modify the initial DAQ system in the lab for future sensor additions and compute the truck's gross vehicle and axle weight. In this system, the DT9829 device and the QuickDAQ program were used to receive the data on the laptop and convert them into Excel files.

Fig 4.7. DT9829, the portable data acquisition multi-sensor measurement device

The twisted cable was used for attaching the geophone to DT9829, as shown in Fig 4.8. the same as the cable in the axle spacing calculation part in the field.

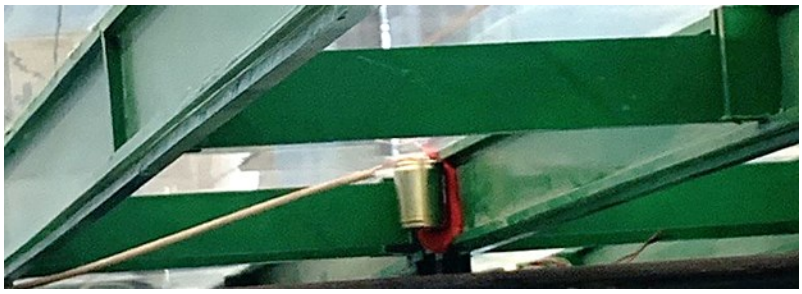

Fig 4.8. The geophone was attached to the device through a twisted cable

Strain gauges were also attached to the breadboard to connect to the DT9829 for separate related studies. As indicated in Fig 4.9. the breadboard was connected to the power supply from the other side. Then all four girders' strain gauges in the closest transverse section to the geophone site were hooked to the DT9829 via breadboard, as shown in Fig 4.10.

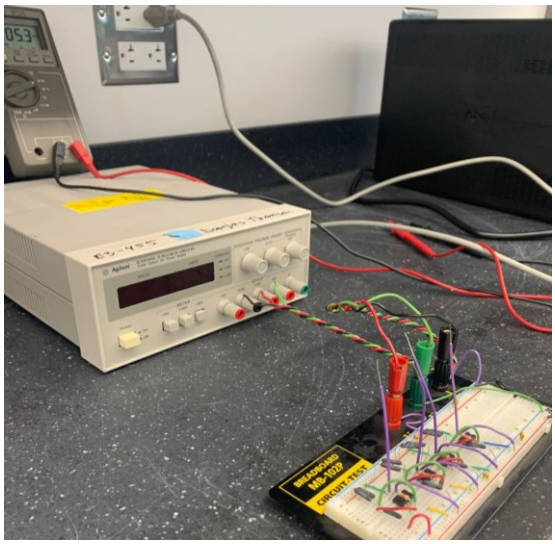

Fig 4.9. The breadboard was attached to the power supply with a voltage of – 6.5 volts while receiving signals

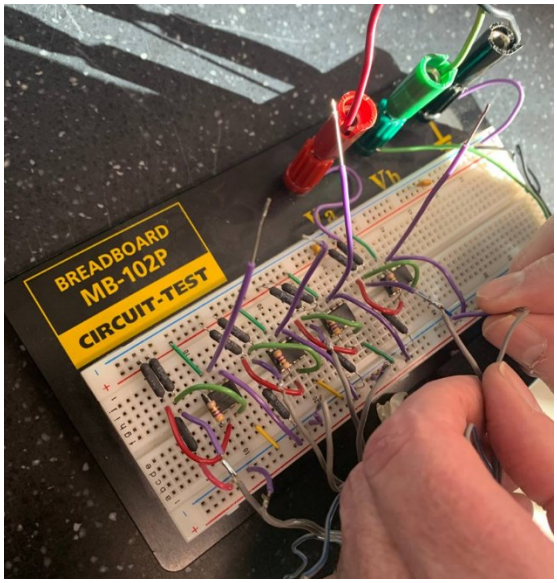

Fig 4.10. The breadboard MB-102P was connected to the four strain gauge wires.

The breadboard with strain gauges was then connected to the DT9829.

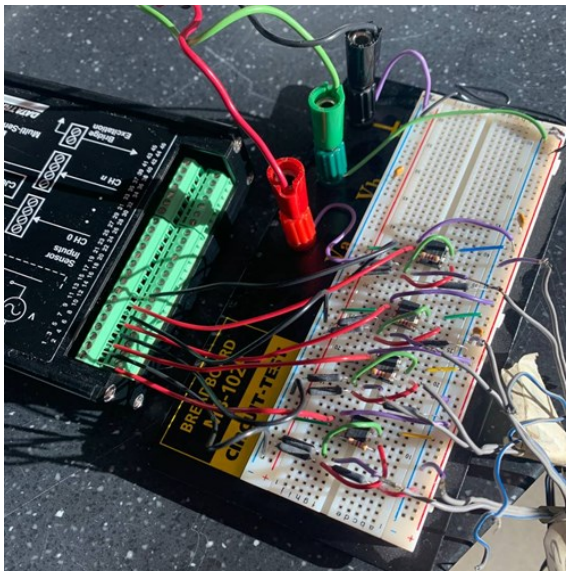

Fig 4.11. Each strain gauges wire was connected to the TD9829 device

TD9829 was connected to the laptop through a USB wire. For reading the data from the system, as the model truck passed the main middle span of the model bridge, the QuickDAQ software was used. Fig 4.12. represents the initial strain gauge data and the environment of the software.

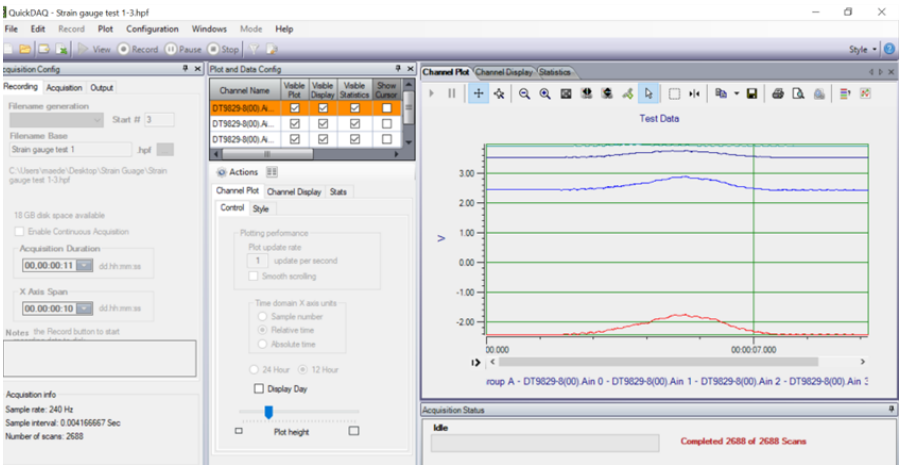

Fig 4.12. QuickDAQ software environment and initial four strain gauges data

After receiving the primary signals, the geophone twisted cable was attached to DT9829.

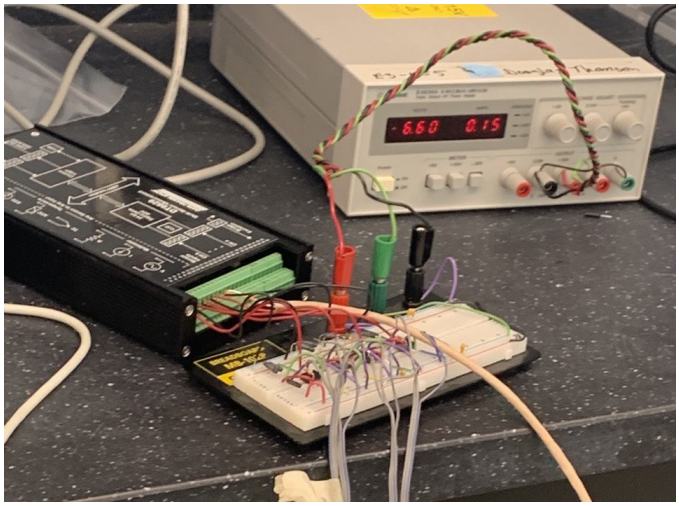

Fig 4.13. The DAQ system with the attached geophone cable

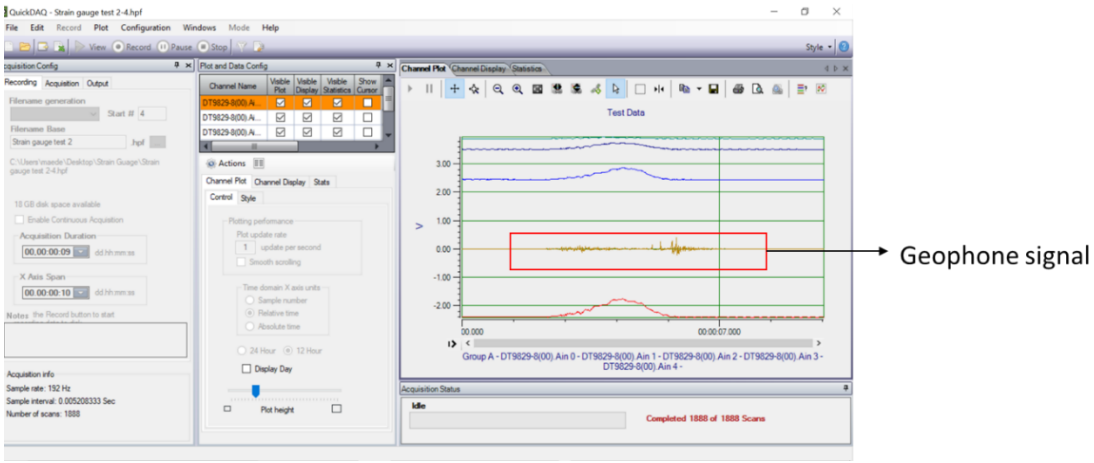

Fig 4.14. Receiving the geophone signal in the QuickDAQ Software

QuickDAQ software received the signals and converted them to an excel file. After obtaining the excel data, the signals were ready to filter and processed to determine the axle positions and model truck configuration.

4.3 Detecting the configuration and axle number of the model truck

After establishing the system for data collection, the test was run for several datasets to obtain the velocity and axle spacings for the model truck. This study's model vehicle has four axles (Figure 4.15. In the truck model, the measured front-to-back axle distance is 0.76 m.

Fig 4.15. The model truck that was used in the laboratory test

4.4 Results and Calculating the Velocity of the Model Truck

The same field methodology was used to calculate the truck's velocity in the laboratory tests. After filtering and converting the units from voltage to velocity, signals were ready for analysis. Fig 4.16. demonstrates the example of the geophone signal in the laboratory. The two locations of the expansion joints where the truck axles enter and depart the bridge are shown in Fig 4.16. The geophone velocity was determined by subtracting the time between the first axle entering and exiting the span. In this example truck enters the span at T1, crosses the first expansion joint, and exits the span at T2. The velocity was computed by dividing the distance between the expansion joints by the time difference. The velocity computed in this case was 1.57 (m/s).

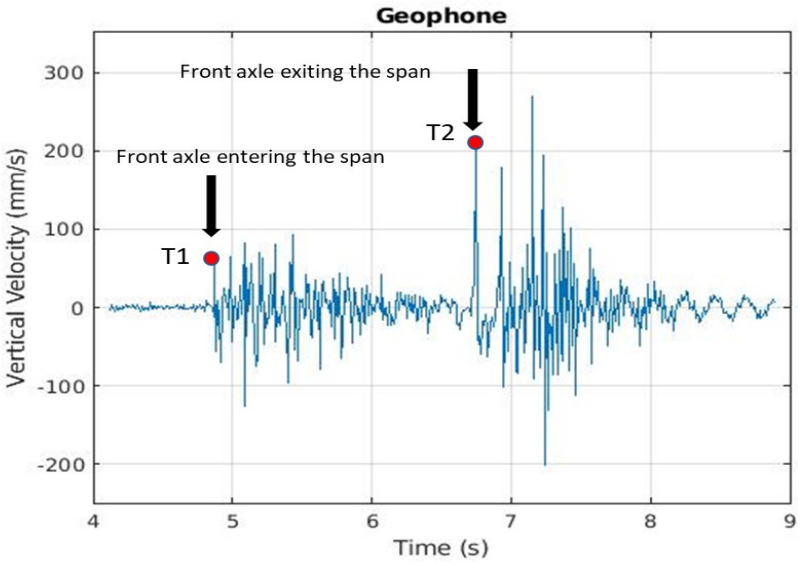

Fig 4.16. The example of the model truck's geophone signal in the laboratory.

Table 4.1 Geophone Velocity Results in the Lab

Set number	Geophone velocity (m/s)
Set 1	1.43
Set 2	1.41
Set 3	1.44
Set 4	1.46
Set 5	1.44
Set 6	1.57
Set 7	1.50

4.4.1 Velocity Validation in the laboratory using two geophones

Two geophones were used in the lab to validate the geophone repeating behaviour, which displays the location of the expansion joints and detects the positions of the axles as well as the times the truck entered and exited the span. The geophones were attached to the model girder under two expansion joints, as shown in Fig 4.17.

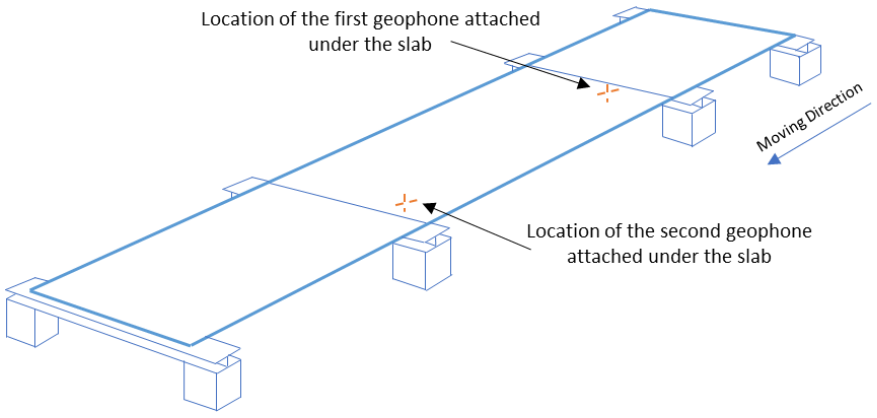

Fig 4.17. Represents the location of two geophones in the bridge model

The axle detection signals produced by the two geophones used in the laboratory test are shown in Fig 4.18. The signals illustrate the locations of the two expansion joint sections where the truck axles enter and exit the span. The red and blue signals had some delays at the beginning and ending points, as seen in Fig 4.18. The distance between the two geophones brought on this slight delay between the two signals. Each geophone responds when the truck enters and when it leaves the span. Therefore, only one is needed to calculate the velocity and detect the entry and departure of the truck.

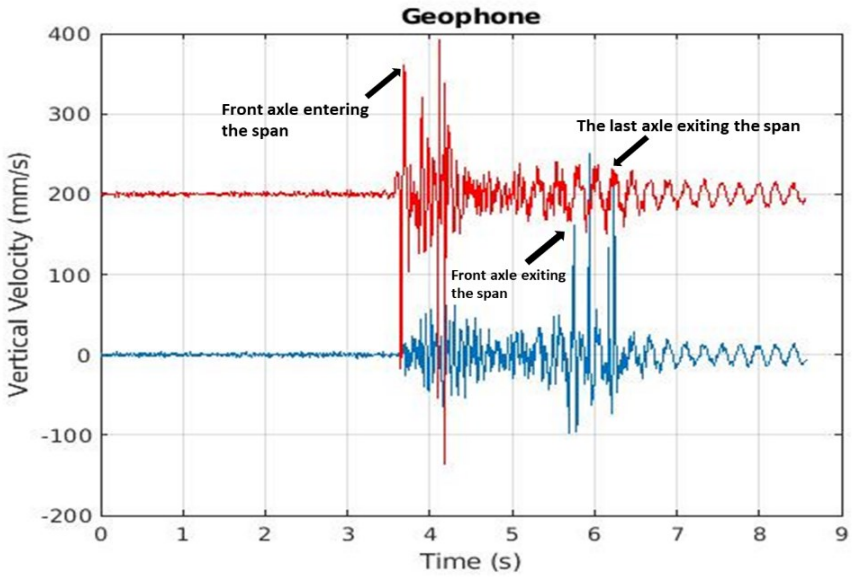

Fig 4.18. The red signal is for the geophone attached to the entering expansion joint, and the blue signal is for the geophone attached to the exiting expansion joint

Observing signals from the two geophones allows for detecting the truck's front axle for calculating the velocity when it passes through the span. With the help of the other geophone, which was attached under the first expansion joint, it was determined that detecting the entering positions where the axles get into the span is correct, as the signals from both

geophones start and end simultaneously. Based on the more significant magnitude signal related to the axles, the position of the geophones and other axles can also be detected.

4.5 Calculating the axle spacings and Results

Similar to how axle spacing was determined in the field section, the computation of axle spacings considers the second part of the signal associated with the location of the second expansion joint when the axle leaves the span. After the velocity estimation, the axle spacings of the model trucks were calculated based on each dataset's velocity. Fig 4.19. shows the measured axle spacings of the model truck.

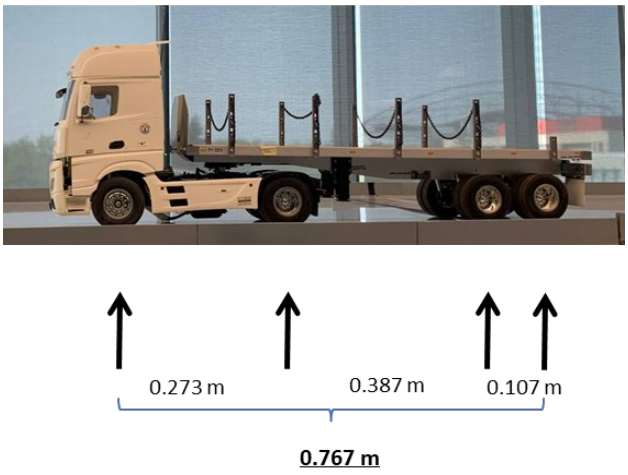

Fig 4.19. Measured axle spacings in the model truck

The geophone signals were used to calculate when each axle departed the span. Figure 4.20. illustrates the lab's model truck with four axles geophone signal. Red dots are used to identify each axle. The distance between each axle was computed by recording the velocity and time at each site. The Front- back axle estimation was 0.75 (m) in this example.

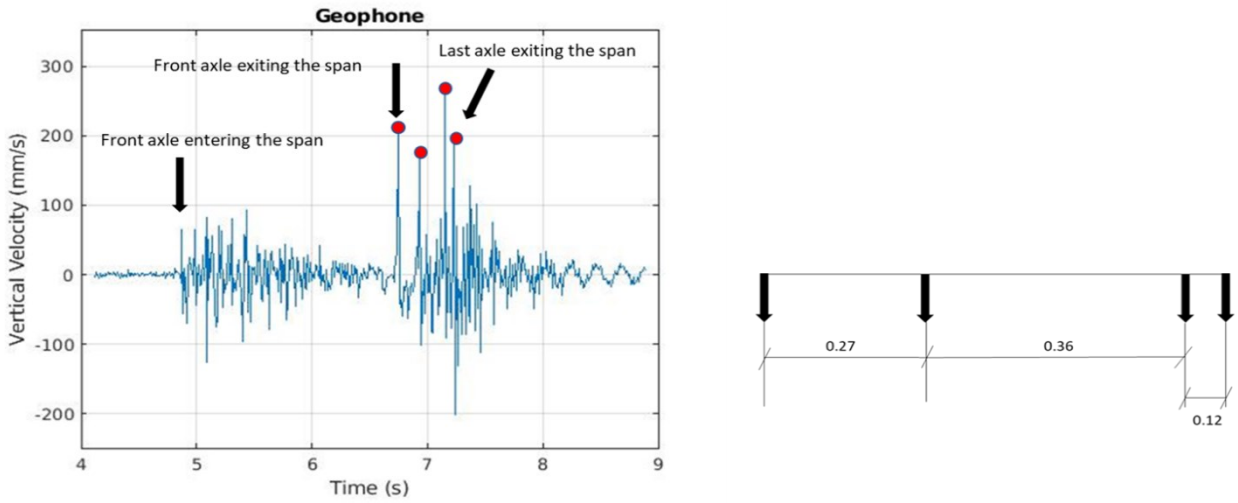

Fig 4.20. Example of axle spacings calculation for one dataset with the velocity of 1.57 (m/s)

Table 4.2. Geophone Axle spacing Results in the Lab

Set number	Front-back axle spacing (1-4) (m)	1-2 (m)	2-3 (m)	3-4 (m)
Set 1	0.76	0.27	0.38	0.11
Set 2	0.73	0.25	0.38	0.10
Set 3	0.76	0.27	0.37	0.12
Set 4	0.71	0.24	0.37	0.10
Set 5	0.74	0.26	0.38	0.10
Set 6	0.75	0.27	0.37	0.11
Set 7	0.79	0.28	0.40	0.11

The truck's velocity, the number of axles, configuration, and axle spacings were calculated as laboratory test results. Some errors were caused due to the sampling rate, and structural response varies from truck to truck. The sampling rate needs to be high enough to capture the rise and fall of the geophone signal accurately, and there might also be variations as the wheel leaves and enters the span.

The geophone could accurately calculate the axle spacing of the model truck in the laboratory. The total data received from 7 datasets in the lab has the mean=0 and SD= 0.01.

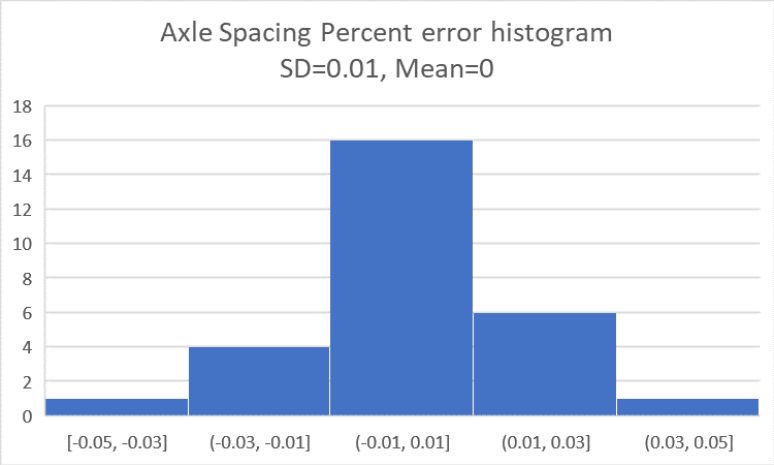

Fig 4.21. The percent error histogram for the axle spacing calculation in the lab

The geophone precisely calculated the lab-based truck model's axle spacings. As a result of the field and laboratory experiment results, the geophone can be utilized as an axle detector in bridge weigh-in-motion systems.

5. Conclusion

This chapter will summarize the essential research findings concerning the research objectives, questions, value, and contribution. It will also review the study's limitations and propose opportunities for future research.

This study aimed to investigate observing the configuration of the truck by assessing the velocity, axle numbers, positions, and axle spacings of the moving trucks using a geophone sensor. According to the results presented at the end of chapters three and four in the field and lab, the geophone can be used as a novel axle detector sensor in the bridge weigh-in-motion system. This can be used to improve axle weight estimates from a BWIM system. The potential future use of this approach is that employing the geophone may significantly enhance computation accuracy since it provides direct velocity information of the bridge reaction, which was the vertical displacement of the bearings in this research. Detecting the exact local events, which are acquiring the exact positions of the axles, velocity, and axle distances can be combined with the gross vehicle weight of the trucks calculated by weighing sensors to compute the individual axle weights of the heavy trucks that travel over the bridges. The research's primary goal is to increase the accuracy of live load assessment, which directly affects the bridges' strength and load-bearing capacity assessment. Many experiments were carried out in the field and the laboratory to evaluate and justify the velocity and axle spacings of the trucks using the geophone sensors. The geophone data was used to estimate velocity and axle spacings for over 90 trucks in the field and was validated with the video camera measurements. The velocity and the geophone signal behaviour were also validated in the lab

with the model bridge using two geophone sensors under each expansion joint. It is also verified with the video camera in two ways in the field with the actual bridge, as represented in chapter three.

The geophone results were validated using two camera positions. One could directly observe the truck passing over the expansion joints, but it was less accurate due to the angle of the images. In the second method, side-view images of the trucks that exited the bridge were used to estimate velocity. The result from the first velocity comparison for over 35 vehicles has a mean error of 1.9% and a standard deviation of 4.6%. The results from the second velocity approach for over 45 vehicles had an error with a mean of 0.8% and a standard deviation of 1.53%. Based on the velocity calculation, the axle spacings were also estimated and verified with a video Camera for 51 trucks in the field. For the distances between the front axle and all other axles, the mean error was equal to 0.1 % and the standard deviation of 1.53%. The mean and standard deviation of the error for the pairs of wheels group (distances less than 2 m) were 0.42 % and 1.4 %, respectively. Finally, for the group containing all possible combinations of axles spacings, standard deviations of 0.29 % and 1.53 % of the error. Based on the comparison results in the velocity and axle spacings calculations, the geophone could estimate and detect the local events with reasonably high accuracy. The calculations in this study were verified with different verification approaches, and the results clearly illustrate that employing the geophone as an axle detector could significantly improve the accuracy of the BWIM system in detecting truck identifications more precisely. Alternatively, utilizing more accurate and intelligent camera technology can help to enhance the measurements and reduce the existing error even more. Further experiments should be conducted to use and combine the results of axle

spacings and velocity calculated in this research with the gross vehicle weight of the trucks to complete the computation of individual axle weights of the trucks travelled over the bridges.

6. REFERENCE

Algohi, B., Mufti, A., & Thomson, D. (2018). Detection of speed and axle configuration of moving vehicles using acoustic emission. *Journal of Civil Structural Health Monitoring*, *8*(3), 353–362. https://doi.org/10.1007/s13349-018-0281-8

Bahrani, N., Blanc, J., Hornych, P., & Menant, F. (2020). Alternate method of pavement assessment using geophones and accelerometers for measuring the pavement response. *Infrastructures*, *5*(3). https://doi.org/10.3390/infrastructures5030025

Bao, T., Babanajad, S. K., Taylor, T., & Ansari, F. (2016). Generalized Method and Monitoring Technique for Shear-Strain-Based Bridge Weigh-in-Motion. *Journal of Bridge Engineering*, *21*(1), 04015029. https://doi.org/10.1061/(asce)be.1943-5592.0000782

Carraro, F., Gonçalves, M. S., Lopez, R. H., Miguel, L. F. F., & Valente, A. M. (2019). Weight estimation on static B-WIM algorithms: A comparative study. *Engineering Structures*, *198*(December 2018), 109463. https://doi.org/10.1016/j.engstruct.2019.109463

Chatterjee, P., OBrien, E., Li, Y., & González, A. (2006). Wavelet domain analysis for identification of vehicle axles from bridge measurements. *Computers and Structures*, *84*(28), 1792–1801. https://doi.org/10.1016/j.compstruc.2006.04.013

Chen, Z., Chan, T. H. T., Nguyen, A., & Yu, L. (2019). Identification of vehicle axle loads from bridge responses using preconditioned least square QR-factorization algorithm. *Mechanical Systems and Signal Processing*, *128*, 479–496. https://doi.org/10.1016/j.ymssp.2019.03.043

Christian, D. S., P, A., & Piggot. (2015). Provided by the author(s) and University College Dublin Library in accordance with publisher policies. Please cite the published version when

available. *Psychology of Sport & Exercise*, *16*, 3–14.

Deng, L., He, W., Yu, Y., & Cai, C. S. (2018). Equivalent Shear Force Method for Detecting the Speed and Axles of Moving Vehicles on Bridges. *Journal of Bridge Engineering*, *23*(8), 1–13. https://doi.org/10.1061/(asce)be.1943-5592.0001278

Dowling, J., Obrien, E. J., & González, A. (2012). Adaptation of Cross Entropy optimisation to a dynamic Bridge WIM calibration problem. *Engineering Structures*, *44*, 13–22. https://doi.org/10.1016/j.engstruct.2012.05.047

Faraz, S. (2020). *Experimental and Field Investigation of a Bridge- Weigh-in-Motion (BWIM) System*.

González, A., and O'Brien, E. J. (1998). "The development of a dynamic bridge weigh-in-motion algorithm." *Pre-Proc., 2nd European Conf. on Weigh-in-Motion of Road Vehicles, E. J. O'Brien and B. Jacob, Eds., European Commission, Luxembourg, 445–452*.

Hansen P.C. (1994). REGULARIZATION TOOLS: A Matlab package for analysis and solution of discrete ill-posed problems. *Numerical Algorithms*, *6*(I 994), 1–35.

He, W., Deng, L., Shi, H., Cai, C. S., & Yu, Y. (2017). Novel Virtual Simply Supported Beam Method for Detecting the Speed and Axles of Moving Vehicles on Bridges. *Journal of Bridge Engineering*, *22*(4), 1–16. https://doi.org/10.1061/(asce)be.1943-5592.0001019

Helmi, K., Bakht, B., & Mufti, A. (2014). Accurate measurements of gross vehicle weight through bridge weigh-in-motion: A case study. *Journal of Civil Structural Health Monitoring*, *4*(3), 195–208. https://doi.org/10.1007/s13349-014-0076-5

Helmi, K., Taylor, T., Zarafshan, A., & Ansari, F. (2015). Reference free method for real time monitoring of bridge deflections. *Engineering Structures*, *103*, 116–124.

https://doi.org/10.1016/j.engstruct.2015.09.002

Kalhori, H., Makki Alamdari, M., Zhu, X., Samali, B., & Mustapha, S. (2017). Non-intrusive schemes for speed and axle identification in bridge-weigh-in-motion systems. *Measurement Science and Technology*, *28*(2). https://doi.org/10.1088/1361-6501/aa52ec

Kalin, J., Žnidarič, A., & Lavrič, I. (2006). *PRACTICAL IMPLEMENTATION OF NOTHING-ON-THE-ROAD BRIDGE WEIGH-IN-MOTION SYSTEM*.

Law, S. S., & Fang, Y. L. (2001). Moving force identification: Optimal state estimation approach. *Journal of Sound and Vibration*, *239*(2), 233–254. https://doi.org/10.1006/jsvi.2000.3118

Liu, H., & Yu, L. (2019). Sparse regularization for traffic load monitoring using bridge response measurements. *Measurement: Journal of the International Measurement Confederation*, *131*(April 2018), 173–182. https://doi.org/10.1016/j.measurement.2018.07.044

Lydon, M., Robinson, D., Taylor, S. E., Amato, G., Brien, E. J. O., & Uddin, N. (2017). Improved axle detection for bridge weigh-in-motion systems using fiber optic sensors. *Journal of Civil Structural Health Monitoring*, *7*(3), 325–332. https://doi.org/10.1007/s13349-017-0229-4

Lydon, M., Taylor, S. E., Robinson, D., Mufti, A., & Brien, E. J. O. (2016). Recent developments in bridge weigh in motion (B-WIM). *Journal of Civil Structural Health Monitoring*, *6*(1), 69–81. https://doi.org/10.1007/s13349-015-0119-6

MacLeod, E., & Arjomandi, K. (2022a). Enhanced Bridge Weigh-in-Motion System Using Hybrid Strain–Acceleration Sensor Data. *Journal of Bridge Engineering*, *27*(9), 1–13. https://doi.org/10.1061/(asce)be.1943-5592.0001924

MacLeod, E., & Arjomandi, K. (2022b). Enhanced Bridge Weigh-in-Motion System Using Hybrid Strain–Acceleration Sensor Data. *Journal of Bridge Engineering*, *27*(9).

https://doi.org/10.1061/(asce)be.1943-5592.0001924

Maros, H., & Juniar, S. (2016). *ON THE USE OF BRIDGE WEIGH-IN-MOTION FOR OVERWEIGHT TRUCK ENFORCEMENT Jim*. *1*, 1–23.

McCrum, D., O'Brien, E., & Khan, M. (2018). Bridge Health Monitoring Using an Acceleration-Based Bridge Weigh-in-Motion System. *Civil Engineering Research in Ireland CERI 2018*, *August*, 84–87.

Moses, F. (1979). Weigh-in-motion system using instrumented bridges. *Tation Engineering Journal of ASCE, 105(3), 233-249.*

Mufti, A., & Helmi, K. (2019). A case for structural health monitoring (SHM) and civionics enhances the evaluation of the load carrying capacity of aging bridges. *Innovative Infrastructure Solutions*, *4*(1), 1–10. https://doi.org/10.1007/s41062-018-0187-7

Mustafa, S., Sekiya, H., Hirano, S., & Miki, C. (2021a). Iterative linear optimization method for bridge weigh-in-motion systems using accelerometers. *Structure and Infrastructure Engineering*, *17*(9), 1245–1256. https://doi.org/10.1080/15732479.2020.1802490

Mustafa, S., Sekiya, H., Hirano, S., & Miki, C. (2021b). Iterative linear optimization method for bridge weigh-in-motion systems using accelerometers. *Structure and Infrastructure Engineering*, *17*(9), 1245–1256. https://doi.org/10.1080/15732479.2020.1802490

O'Brien, E. J., Znidaric, A., & Dempsey, A. T. (1999). Comparison of two independently developed bridge weigh-in-motion systems. *Heavy Vehicle Systems*, *6*(1), 147–161. https://doi.org/10.1504/ijhvs.1999.054503

O'Brien, E., Žnidarič, A., & Ojio, T. (2013). Bridge weigh-in-motion - latest developments and applications world wide. *International Conference on Heavy Vehicles HVParis 2008*, *April*,

39–56. https://doi.org/10.1002/9781118623305.ch2

Obrien, E. J., González, A., & Dowling, J. (2010). A filtered measured influence line approach to Bridge Weigh-in-Motion. *Bridge Maintenance, Safety, Management and Life-Cycle Optimization - Proceedings of the 5th International Conference on Bridge Maintenance, Safety and Management*, *July*, 965–972. https://doi.org/10.1201/b10430-137

Ojio, T., Carey, C. H., OBrien, E. J., Doherty, C., & Taylor, S. E. (2016). Contactless Bridge Weigh-in-Motion. *Journal of Bridge Engineering*, *21*(7), 04016032. https://doi.org/10.1061/(asce)be.1943-5592.0000776

Oskoui, E. A., Taylor, T., & Ansari, F. (2020). Method and sensor for monitoring weight of trucks in motion based on bridge girder end rotations. *Structure and Infrastructure Engineering*, *16*(3), 481–494. https://doi.org/10.1080/15732479.2019.1668436

Richardson, J., Jones, S., Brown, A., O'Brien, E., & Hajializadeh, D. (2014a). On the use of bridge weigh-in-motion for overweight truck enforcement. *International Journal of Heavy Vehicle Systems*, *21*(2), 83–104. https://doi.org/10.1504/IJHVS.2014.061632

Richardson, J., Jones, S., Brown, A., O'Brien, E., & Hajializadeh, D. (2014b). On the use of bridge weigh-in-motion for overweight truck enforcement. *International Journal of Heavy Vehicle Systems*, *21*(2), 83–104. https://doi.org/10.1504/IJHVS.2014.061632

Rowley, C. W., OBrien, E. J., Gonzalez, A., & Žnidarič, A. (2009). Experimental testing of a moving force identification bridge weigh-in-motion algorithm. *Experimental Mechanics*, *49*(5), 743–746. https://doi.org/10.1007/s11340-008-9188-3

Sekiya, H. (2019). Field Verification over One Year of a Portable Bridge Weigh-in-Motion System for Steel Bridges. *Journal of Bridge Engineering*, *24*(7), 04019063.

https://doi.org/10.1061/(asce)be.1943-5592.0001411

Sekiya, H., Kubota, K., & Miki, C. (2018a). Simplified Portable Bridge Weigh-in-Motion System Using Accelerometers. *Journal of Bridge Engineering*, *23*(1), 1–15. https://doi.org/10.1061/(asce)be.1943-5592.0001174

Sekiya, H., Kubota, K., & Miki, C. (2018b). Simplified Portable Bridge Weigh-in-Motion System Using Accelerometers. *Journal of Bridge Engineering*, *23*(1), 04017124. https://doi.org/10.1061/(asce)be.1943-5592.0001174

Wang, H., Nagayama, T., Zhao, B., & Su, D. (2017). Identification of moving vehicle parameters using bridge responses and estimated bridge pavement roughness. *Engineering Structures*, *153*, 57–70. https://doi.org/10.1016/j.engstruct.2017.10.006

Wang, N. B., Ren, W. X., & Chen, Z. W. (2017). Wavelet-based automatic identification method of axle distribution information. *Structural Engineering and Mechanics*, *63*(6), 761–769. https://doi.org/10.12989/sem.2017.63.6.761

Wu, S. Q., & Law, S. S. (2010). Moving force identification based on stochastic finite element model. *Engineering Structures*, *32*(4), 1016–1027. https://doi.org/10.1016/j.engstruct.2009.12.028

Yu, L., & Chan, T. H. T. (2007). Recent research on identification of moving loads on bridges. *Journal of Sound and Vibration*, *305*(1–2), 3–21. https://doi.org/10.1016/j.jsv.2007.03.057

Yu, Y., Cai, C. S., & Deng, L. (2016a). State-of-the-art review on bridge weigh-in-motion technology. *Advances in Structural Engineering*, *19*(9), 1514–1530. https://doi.org/10.1177/1369433216655922

Yu, Y., Cai, C. S., & Deng, L. (2016b). State-of-the-art review on bridge weigh-in-motion

technology. In *Advances in Structural Engineering* (Vol. 19, Issue 9, pp. 1514–1530). SAGE Publications Inc. https://doi.org/10.1177/1369433216655922

Yu, Y., Cai, C. S., & Deng, L. (2017a). Vehicle axle identification using wavelet analysis of bridge global responses. *JVC/Journal of Vibration and Control*, *23*(17), 2830–2840. https://doi.org/10.1177/1077546315623147

Yu, Y., Cai, C. S., & Deng, L. (2017b). Vehicle axle identification using wavelet analysis of bridge global responses. *JVC/Journal of Vibration and Control*, *23*(17), 2830–2840. https://doi.org/10.1177/1077546315623147

Zhao, H., & Uddin, N. (2010). Algorithm to identify axle weights for an innovative BWIM system-Part II. *IABSE-JSCE Joint Conference on Advances in Bridge Engineering*, *1979*, 978–984.

Zhao, H., Uddin, N., O'Brien, E. J., Shao, X., & Zhu, P. (2014). Identification of Vehicular Axle Weights with a Bridge Weigh-in-Motion System Considering Transverse Distribution of Wheel Loads. *Journal of Bridge Engineering*, *19*(3), 04013008. https://doi.org/10.1061/(asce)be.1943-5592.0000533

Zhao, H., Uddin, N., Shao, X., Zhu, P., & Tan, C. (2015). Field-calibrated influence lines for improved axle weight identification with a bridge weigh-in-motion system. *Structure and Infrastructure Engineering*, *11*(6), 721–743. https://doi.org/10.1080/15732479.2014.904383

Zhu, X. Q., & Law, S. S. (2001). Orthogonal function in moving loads identification on a multi-span bridge. *Journal of Sound and Vibration*, *245*(2), 329–345. https://doi.org/10.1006/jsvi.2001.3577